UNIVERSIDAD NACIONAL AUTÓNOMA DE MEXICO

PROGRAMA DE POSGRADO EN ASTROFÍSICA
INSTITUTO DE ASTRONOMÍA

CHARACTERIZATION OF HIGH-ENERGY ASTROPHYSICAL SOURCES VIA THERMALLY-PRODUCED NEUTRINO PROPERTIES

TESIS
QUE PARA OPTAR POR EL GRADO DE:
DOCTOR EN CIENCIAS
(ASTROFÍSICA)

PRESENTA:
GIBRÁN MORALES RIVERA

TUTOR PRINCIPAL
DR. NISSIM ILLICH FRAIJA CABRERA
INSTITUTO DE ASTRONOMÍA, UNAM

MIEMBROS DEL COMITÉ TUTOR
DR. DANY PIERRE PAGE ROLLINET
INSTITUTO DE ASTRONOMÍA, UNAM

DR. DIEGO LÓPEZ CÁMARA RÁMIREZ
INSTITUTO DE ASTRONOMÍA, UNAM

CIUDAD UNIVERSITARIA, CIUDAD DE MÉXICO, JULIO DE 2022

Universidad Nacional Autónoma
de México

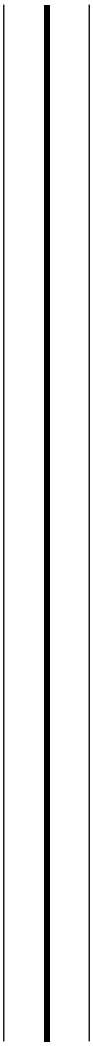

Instituto de Astronomía

Characterization of high-energy astrophysical sources via thermally-produced neutrino properties

Gibrán Morales Rivera

A dissertation submitted
for the degree of:

Doctor of Philosophy

Supervisor:
Dr. Nissim Illich Fraija Cabrera

Mexico City, July 2022

Hoja de datos del jurado

1. **Datos del alumno**
   Morales
   Rivera
   Gibrán
   gmorales@astro.unam.mx
   Universidad Nacional Autónoma de México
   Instituto de Astronomía
   309162861

2. **Datos del tutor**
   Dr.
   Nissim Illich
   Fraija
   Cabrera

3. **Datos del sinodal 1**
   Dr.
   Antonio
   Marinelli

4. **Datos del sinodal 2**
   Dr.
   Christian
   Giovanny
   Bernal

5. **Datos del sinodal 3**
   Dr.
   Hermes
   León
   Vargas

6. **Datos del sinodal 4**
   Dr.
   Dany Pierre
   Page
   Rollinet

7. **Datos del sinodal 5**
   Dra.
   Catalina
   Espinoza
   Hernández

8. **Datos del trabajo**
   Characterization of high-energy astrophysical sources via thermally-produced neutrino properties
   51 pp.
   2022

To my parents

This page has been intentionally left blank.

Acknowledgments

I want to thank God for putting the right people in my life. First of all, I want to thank my parents for their unconditional love and affection that have allowed me to become the person I am today. This thesis is the culmination of an academic formation that started when you began to educate me from an early age. You are the example that everything can be achieved by fighting and persevering daily. You are my true heroes in real life.

I thank my siblings and their respective families (in order of appearance: Omar, Wendy, Horte, Carlos, Jalil, Hannia, Hiram, Charlie, Derek) because you complement my unique family nucleus and fill me with happiness, my grandmother Magdalena and my grandmother Maria who during this period reached my two grandparents in heaven (Thy word is a lamp unto my feet, and a light unto my path).

I thank Nina for having accompanied me throughout this journey, patience, and for supporting me in good and bad times. Do you already know which is your favorite planet?

I especially want to thank Dr. Nissim for his guidance and direction. Six years that I have had the privilege of being able to work with you and for the advice and life teachings that go beyond academics. I would also like to thank my Tutorial Committee, formed by Dr. Dany Page and Dr. Diego López Cámara, for guiding me throughout this process.

To the kind reader, I am going to tell you a secret that only my immediate family knows. I did not finish kindergarten. The reason is that at the end of my second year, I got sick with chicken pox and stopped attending. My parents enrolled me the following school year in elementary school, but I should have been in the third grade. Since then, I have lived in constant fear (tormented by my brother Omar) that my further studies will be invalidated by the simple fact that I never graduated from kindergarten. I hope that the Ph.D. will not be the exception.

I thank the Instituto de Astronomía and all the staff working within its facilities for providing me with the optimal space and services for my graduate studies to be carried out. I am also very grateful to my alma mater, UNAM, because I have spent more than half of my life in

your classrooms since August 2008, when I met you for the first time. You are indeed a source of pride for our country and for me. This thesis and my graduate studies were funded by a CONACyT doctoral grant 825482 and the UNAM-DGAPA-PAPIIT program IN106521.

THANK YOU!

Agradecimientos

Quiero agradecer a Dios por ponerme a las personas indicadas en mi vida. En primer lugar quiero agradecer a mis padres por todo su amor y cariño incondicional que me han permitido formar la persona que soy el día de hoy. Esta tesis es la culminación de una formación académica que empezó desde que ustedes comenzaron a educarme desde temprana edad. Ustedes son el ejemplo de que todo se puede lograr luchando y perseverando día con día. Son mis verdaderos héroes en la vida real.

Agradezco a mis hermanos y sus respectivas familias (por orden de aparición: Omar, Wendy, Horte, Carlos, Jalil, Hannia, Hiram, Charlie, Derek) porque ustedes complementan mi núcleo familiar inigualable y me llenan de felicidad, a mi abuelita Magdalena y a mi abuelita María que durante este período alcanzó a mis dos abuelos en el cielo (Lámpara es a mis pies tu palabra y lumbrera a mi camino).

Agradezco a Nina por haberme acompañado en toda esta travesía, tenerme paciencia y apoyarme en los buenos y malos momentos. ¿Ya sabes cúal es tu planeta favorito?

Especialmente quiero agradecer al Dr. Nissim por su guía y dirección. Seis años que he tenido el privilegio de poder trabajar con usted y por los consejos y enseñanzas de vida que van más allá de lo académico. Agradezco también a mi Cómite Tutor conformado por el Dr. Dany Page y Dr. Diego López Cámara, por haberme orientado y guiado durante todo este proceso.

Al amable lector que está leyendo esto, le voy a contar un secreto que sólo mi familia directa sabe. Yo no acabé el kinder, la razón es que a final de mi segundo año enfermé de varicela y dejé de asistir. El siguiente ciclo escolar mis papás me inscribieron a la primaria, pero realmente debería de haber estado cursando el tercer año. Desde ese momento vivo con un miedo constante (atormentado por mi hermano Omar) de que mis estudios posteriores sean invalidados por el simple hecho de que nunca me gradué del kinder, espero que el doctorado no sea la excepción.

Agradezco al Instituto de Astronomía y a todo el personal que labora dentro de sus insta-

laciones por haberme brindado un espacio y los servicios óptimos para que mis estudios de posgrado se llevaran a cabo. También agradezco enormemente a mi alma máter, la UNAM, porque he pasado más de la mitad de mi vida dentro de tus aulas desde aquel mes de agosto de 2008 que te conocí por primera vez. Realmente eres un orgullo para mi y para la nación. Esta tesis y mis estudios de posgrado se realizaron con el financiamiento de una beca de doctorado CONACyT No. 825482 y del programa UNAM-DGAPA-PAPIIT No. IN106521.

¡GRACIAS!

Characterization of high-energy astrophysical sources via thermally-produced neutrino properties

Gibrán Morales Rivera
Instituto de Astronomía, Universidad Nacional Autónoma de México

Abstract

With the early detection of neutrinos from SN1987A, as well as the recent detection of gravitational waves, astronomy has entered a new era of multi-messenger observation. In this context, neutrinos represent a valuable detection channel for characterizing a variety of astrophysical sources. For example, in this work, we focus primarily on the most energetic electromagnetic events in the Universe, known as gamma-ray bursts (GRB), which generate enormous number of neutrinos through thermal processes. These neutrinos obey the medium's characteristics as they propagate through the associated effective potential. Throughout this research, we have studied how these inherent properties of neutrinos are modified within different material media and what information can be extracted from these types of sources, which during an initial stage are opaque to photons.

Keywords:
–Thermal neutrinos: oscillation, propagation, detection
–Gamma-ray bursts: short GRB, long GRB
–High-energy sources: GRB, Central Compact Objects, Strange Stars
–Progenitors: Magnetar, Black Hole, Neutron star, merger, CCSNe, central engine

Caracterización de fuentes astrofísicas de altas energías a través de las propiedades de neutrinos térmicos

Gibrán Morales Rivera
Instituto de Astronomía, Universidad Nacional Autónoma de México

Resumen

Con la temprana detección de neutrinos provenientes de la SN1987A más la reciente detección de ondas gravitacionales, una nueva rama de observación multi-mensajero en la Astronomía ha surgido. Dentro de este contexto, los neutrinos representan un canal de detección valioso para caracterizar múltiples fuentes astrofísicas, como ejemplo, en este trabajo nos enfocamos en los eventos electromagnéticos mas energéticos que existen en el Universo, los llamados *gamma-ray bursts* (GRBs) en donde una gran cantidad de neutrinos son creados a través de procesos térmicos. Estos neutrinos obedecen las características del medio cuando se propagan a través del potencial efectivo asociado. A lo largo de esta investigación, hemos estudiado como se ven modificadas estas propiedades inherentes a los neutrinos dentro de diferentes medios materiales y que información se puede extraer de este tipo de fuentes, ya que muchas veces son opacas incialmente a los fotones.

Contents

List of Figures

List of Tables

1 Introduction

Throughout human history, mankind has looked into the sky to find answers to the unknowns present here on Earth. Many civilizations developed with a deep understanding of the cosmos. Thus, from pre-Columbian times, the Mayans created their own solar calendar and were able to predict eclipses with their physical eyes alone. However, it was not until 1609 that it was possible to observe a little further with the help of the first telescope built by Galileo.

In this context, the study of neutrinos is a genuinely new field of study, since it is almost 100 years since Wolfgang Pauli first proposed their existence and less than a half-century since the theory of their oscillations was developed. However, their impact on our understanding of our world has been enormous, not only because of the peculiar characteristics they present but also because they have allowed us to observe our Universe through different eyes.

At the moment, many neutrinos cross through our bodies every minute without us even noticing it. Neutrinos are created in various places; some are created close to us, such as the Earth's atmosphere, while others are created far beyond our Galaxy, as in the case of neutrinos produced by extragalactic sources. These neutrinos travel through the intergalactic medium, passing through everything in their path without being disturbed and carrying valuable information from the far reaches of the Universe with them.

A new branch of multi-messenger observation in astronomy has emerged with the early detection of neutrinos from SN1987A plus the recent detection of gravitational waves. Neutrinos represent a valuable detection channel to characterize multiple astrophysical sources. For example, in this work, we focus on the most energetic electromagnetic events in the Universe, the so-called gamma-ray bursts (GRB), where many neutrinos are created through thermal and acceleration processes. The study of neutrinos produced inside a GRB is intriguing because they not only escape the initial burst but do so before the photons themselves. Despite their significance, these high energetic astrophysical events were unknown to us for a long time, only being discovered in the last century. Likewise, we have also studied other types of high-energy sources.

Although much progress has been made in the field of GRB astronomy in recent years, partic-

ularly in the characterization of the progenitors, many questions remain unanswered or need to be clarified further. Nevertheless, we believe that neutrinos can be a crucial messenger for addressing these unknowns, and we have developed this work in that spirit.

The study of neutrino properties, for example, could help us confirm the type of progenitor that causes GRB. Neutrino detectability may also play a role in detecting *off-axis* GRB[1] (Nakar et al., 2002), as well as explaining the origin of a portion of the diffuse astrophysical neutrino flux measured. As a result, we use the multi-messenger nature of GRB to address some of these open questions in this work by examining the evolution of thermal neutrino flavors in various media with or without a strong magnetic contribution. We are particularly interested in those neutrinos with energies in the MeV range produced by thermal processes.

The thesis begins with a literature review of the concepts required to introduce the reader to the field of study and to put the work in context. Throughout this research, we have studied how the inherent properties of neutrinos are modified within different backgrounds and what information can be extracted from each source. We focus our neutrino studies on the winds produced by short gamma-ray bursts (sGRB) events (Article 1), their progenitors (Article 2), and long GRB (LGRB) central engine models (Article 3). However, we have also discussed to a lesser extent other sources of interest, such as central compact objects (CCO) (Articles 4 and 5) and strange stars (SS) (Article 6). Chapter 2 presents a review of the neutrino formalism, focusing on the theory of oscillations and detection. Subsequently, we present in Chapter 3, a brief compilation of the astrophysical sources considered in this work where we discuss, among other things, the primary energy extraction mechanisms and the fireball model. Then, in Chapter 4, we discuss the motivation and methodology for the articles presented at the end of the thesis and the author's contribution to these works. Finally, the general conclusions are grouped in Chapter 5.

Unless otherwise specified, we use the system of natural units where $(k = c = \hbar = 1)$ as well as, the convention of $Q = Q/10^x$ in cgs units for the remainder of this thesis. We have also considered an Einstein-deSitter Universe with parameters $h = 0.673$, $\Omega_\Lambda = 0.685$, and $\Omega_m = 0.315$ (Patrignani et al., 2016), where Ω_Λ represents the dark energy density of the ΛCDM Universe and Ω_m denotes the pressureless matter density.

It is also worth mentioning that the Einstein summation convention will be used in which the $\sum$ symbol is suppressed when two indices are repeated, i.e., if the vector

$$\vec{u} = \sum_{i=1}^{n} u_i x_i \ ,$$

then it is understood that $\vec{u} = u_i x_i$ corresponds to the result of the summation even though it is not explicitly written.

[1] It refers to those events that lack gamma-ray emission due to their line of sight, with only late emission recorded at lower frequencies through the so-called orphan afterglow. They are discussed below

2 Neutrinos

2.1 A brief history of neutrinos

Neutrino physics is a relatively new and active field of research. Neutrinos, along with photons, are the most abundant particles in the Universe. These are the only elementary fermions that do not have an electric charge; as a result, they cannot be influenced by electromagnetic interactions and can only participate through weak interaction processes with bosons ($W^{\pm}$ and Z^0). Considering their effective cross section is so small,[1] a large number of these particles pass through our bodies at all times without our awareness. Because of these specific conditions, their existence was not conceived until the twentieth century, when physicists began to experiment with the phenomenon of radioactivity. The discoveries of Pierre and Marie Currie, and later Rutherford, established the existence of three types of radioactive decays; alpha (α), beta (β), and gamma (γ) radiation. It was not until 1914 when J. Chadwick demonstrated that the spectrum of beta radiation was continuous rather than discrete, which presented an additional problem because energy was not conserved but rather depleted during this quantum transition (see Figure 2.1).

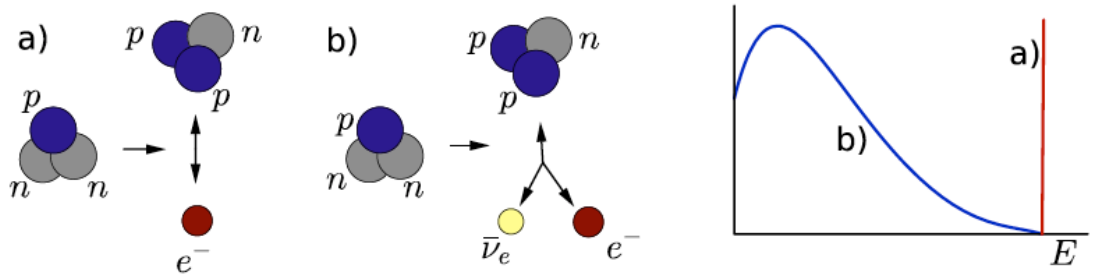

Figure 2.1:
Left: *Tritium $\beta-$decays into (a) an electron + Helium and (b) an electron + Helium + a neutrino.*
Right: *The expected decays are shown for both discrete (a) and continuous (b) scenarios.*

Wolfgang Pauli was the first to recognize that the only way of explaining the continuous beta spectra under the constraint of energy-momentum conservation was to postulate the existence

[1] A typical cross-section is: $\sigma_\nu \sim 10^{-44} \left(\frac{E_\nu}{\mathrm{MeV}}\right) \mathrm{cm}^{-2}$

of a new, neutral particle that was produced in the $\beta-$decay along with the electron and that had not been detected in any experiment before. [2] As a result, in 1930, Pauli wrote a letter to his colleagues gathered in Tübingen, Germany, where he proposed that $\beta-$decay could be explained by a three-body interaction

$$(A, Z) \rightarrow (A, Z+1) + e^- + "n" \ ,$$

the existence of a new fermionic particle "n", that should be electrically neutral, weakly interacting, with small mass, spin $1/2$ and that if found, should be called *neutron*, in analogy to the proton.

Sometime later, Chadwick discovered the neutron, which is still known today by that name. Subsequently, Enrico Fermi suggested the term neutrino (which means 'small neutron' in Italian) to the particle proposed by Pauli, hypothesized that if it existed, it must be a massless particle, and discovered that the probability of its interaction with the matter was practically zero, making the idea of detecting any of these particles absurd at the time.

Later, one of Fermi's students, Bruno Pontecorvo, proposed that it may be possible to detect neutrinos if a large number of them interacted with protons in a scintillator liquid via inverse beta decay (IBD). In practice, Reines and Cowan developed a detector based on a tank filled with Cadmium chloride ($CdCl_2$) and surrounded by photomultipliers (PMT) on its walls. This detector was built at a depth of 12 meters, using neutrinos supplied from the Savannah River nuclear reactor in the United States. The reaction produced a positron, which annihilates with the medium's electrons, resulting in gamma-rays, and a free neutron, which in turn can be captured by a Cadmium atom and again be re-emitted in a single $\gamma-$ray

$$\begin{aligned} p + \bar{\nu}_e \rightarrow \quad & n + e^+ \\ & e^- e^+ \rightarrow \gamma\gamma \\ & n + {}^{108}\mathrm{Cd} \ \rightarrow \ {}^{109}\mathrm{Cd} + \gamma \ . \end{aligned} \tag{2.1}$$

Pontecorvo's predictions came true, and the particle proposed by Pauli was identified for the first time in 1956. Thereafter, the finding of oscillations in the neutral kaon system $K^0 \leftrightarrows \bar{K}^0$ (Gell-Mann & Pais, 1955) encouraged Pontecorvo to propose the same possibility for neutrinos, with oscillations between particle and antiparticle states $\nu \leftrightarrows \bar{\nu}$.

Finally, Cowan and Reines sent Pauli a telegram on June 14, 1956, informing him of their new discovery, which reads: *"We are happy to inform you that we have definitely detected neutrinos ..."* (Reines et al., 1960).

L.M. Lederman, M. Schwartz, and J. Steinberger discovered a second neutrino, the muon neutrino (ν_μ), in 1962 at the Brookhaven National Laboratory in Upton, New York (Danby et al., 1962). It was originally predicted by S. Sakata and T. Inoue in 1946 (Sakata & Inoue, 1955). Almost four decades later, the *Direct Observations of NU Tau* (DONUT) collaboration at FermiLab announced the discovery of the tauonic neutrino (ν_τ) and thus completing

[2] There was also an assumption at the time that energy in $\beta-$decay was not preserved

the three leptonic families within the Standard Model of Particles (SM) (Kodama et al., 2001).

Following that, *Super-Kamiokande*, the experiment that measured the flux of solar neutrinos reaching the Earth, discovered a deficiency of incident neutrinos in comparison to the theoretical models' predictions (the so-called *solar neutrino problem*). One explanation for this shortage is that neutrinos have mass and change flavor on their approach to Earth. Almost at the same time, the *Sudbury Neutrino Observatory* (SNO) also confirmed the existence of the oscillation theory and provided a solution to the solar neutrino problem. The joint confirmation of this phenomenon led to the award of the Nobel Prize in Physics in 2015.

2.2 Neutrino oscillation formalism

The term oscillation refers to a quantum phenomenon in which there is a periodic change in the probability amplitude of an elementary particle created in an eigenstate α and detected in an eigenstate β, with $\alpha \neq \beta$. Although in this work we will restrict ourselves to the study of neutrinos, this phenomenon does not occur exclusively on these particles. In this work, the calculation of the probability of oscillations will be presented following the books of Giunti and Bilenky (Giunti & Kim, 2007; Bilenky, 2010).

A defined neutrino of flavor α and momentum $\vec{p}$ is described in a flavor state as $|\nu_\alpha\rangle$ with $(\alpha = e, \mu, \tau)$ created by the interaction of the weak gauge bosons with the charged leptons. They can be found in a juxtaposition of the so-called "mass" eigenstates as they propagate through space $|\nu_a\rangle$ (with $a = 1, 2, 3$), [3] which evolve, so that a neutrino created with a flavor α can be detected with a different flavor β (Pontecorvo, 1968; Barger et al., 1980), this can be stated mathematically as:

$$|\nu_\alpha\rangle = \sum_{a=1}^{3} U^*_{\alpha a} |\nu_a\rangle \ , \tag{2.2}$$

i.e., using the unitary matrices U^* and U,[4] flavor eigenstates are defined in terms of mass eigenstates and vice versa. Assuming a plane wave approximation, the Schrödinger equation $i\,|\dot{\nu}_\alpha(t)\rangle = \mathcal{H}_f\,|\nu_\alpha(t)\rangle$ governs the temporal evolution of neutrinos, whose solution is given by

$$|\nu_\alpha(t)\rangle = e^{-i\mathcal{H}_f t}\,|\nu_\alpha(0)\rangle = \mathcal{U}_f(t)\,|\nu_\alpha(0)\rangle \ , \tag{2.3}$$

with $\mathcal{H}_f$ the hamiltonian and $\mathcal{U}_f$ the temporal evolution operator in a flavor basis and where the unitary matrix has the following entries

$$U = (U_{\alpha a}) = \begin{pmatrix} U_{e1} & U_{e2} & U_{e3} \\ U_{\mu 1} & U_{\mu 2} & U_{\mu 3} \\ U_{\tau 1} & U_{\tau 2} & U_{\tau 3} \end{pmatrix} . \tag{2.4}$$

[3] It is worth mentioning that the notation of Greek letters in literature refers to "flavor" eigenstates. For mass eigenstates, on the other hand, Latin characters are employed.

[4] This unitary matrix is known as the *Pontecorvo–Maki–Nakagawa–Sakata* (PMNS) matrix in a three-flavor mixing scenario (Maki et al., 1962; Gross & Wilczek, 1974).

$U = U(\theta_1, \theta_2, \theta_3)$ is often parametrized as

$$U = \begin{pmatrix} C_2C_3 & S_3C_2 & S_2 \\ -S_3C_1 - S_1S_2C_3 & C_1C_3 - S_1S_2S_3 & S_1C_2 \\ S_1S_3 - S_2C_1C_3 & -S_1C_3 - S_2S_3C_1 & C_1C_2 \end{pmatrix}, \tag{2.5}$$

where $S_i \equiv \sin\theta_i$ and $C_i \equiv \cos\theta_i$ for $i = 1, 2, 3$. The values θ_i are the mixing angles in the vacuum. To refer to these angles, sometimes the following notations are used

$$\theta_{23} = \theta_1, \quad \theta_{13} = \theta_2, \quad \theta_{12} = \theta_3 \ .$$

The Hamiltonian for neutrino propagation in vacuum is diagonal in the mass eigenstate basis and is defined as

$$\mathcal{H}_m = \begin{pmatrix} E_1 & 0 & 0 \\ 0 & E_2 & 0 \\ 0 & 0 & E_3 \end{pmatrix}, \tag{2.6}$$

where $E_a = \sqrt{m_a^2 + \mathbf{p}^2}$, $a = 1, 2, 3$, are the neutrino energies for the mass eigenstates $|a\rangle$, $a = 1, 2, 3$ with masses m_a, $a = 1, 2, 3$. Note that we assume the momentum $\mathbf{p}$ to be the same for all mass eigenstates. It is worth noting that the bases $\mathcal{H}_f$ and $\mathcal{H}_m$ are simply two distinct representations of the same Hilbert space but it is more feasible to work on a mass eigenstate basis where $\mathcal{H}_f$ is diagonal rather than a flavor basis where it is not. Therefore, we employ the unitary matrix to perform the basis transformation, such as,

$$\mathcal{H}_m = U^{-1}\mathcal{H}_f U \ . \tag{2.7}$$

Then, the transition probability amplitude that a neutrino in a flavor eigenstate α will be detected with a flavor β after traveling for a time t is defined as

$$\mathcal{A}_{(\nu_\alpha \to \nu_\beta)}(t) \equiv \langle \nu_\beta | \nu(t) \rangle = \langle \nu_\beta | \mathcal{U}_f(t) | \nu_\alpha \rangle = \sum_{a=1}^{n} \sum_{b=1}^{n} U^*_{\alpha a} U_{\beta b} e^{-i(\mathcal{H}_{m,b} - \mathcal{H}_{m,a})\ t} \langle \nu_b | \nu_a \rangle \ , \tag{2.8}$$

and it follows that

$$\begin{aligned} \mathcal{A}_{\nu_\alpha \to \nu_2 \beta}(t) &\equiv \sum_{a=1}^{n} \sum_{b=1}^{n} U^*_{\alpha a} U_{\beta b} e^{-i(\mathbf{p}_b - \mathbf{p}_a)\ L} \delta_{ba} \\ &= \sum_{a=1}^{n} U^*_{\alpha a} U_{\beta a} e^{-i(p_a - E_a)\ L} \\ &= \sum_{a=1}^{n} U^*_{\alpha a} U_{\beta a} e^{-i(p_a - p_a - (m_a^2/2p_a))\ L} \\ &= \sum_{a=1}^{n} U^*_{\alpha a} U_{\beta a} e^{i\frac{m_a^2 L}{2E_a}} \ , \end{aligned} \tag{2.9}$$

where we have assumed that neutrinos propagate at relativistic velocities $|\mathbf{p}_a| \gg m_a$ and the following approximations are fulfilled:

- $L \approx t$
- $E \approx p$
- $E_a = \sqrt{m_a^2 + \mathbf{p}_a^2} = p_a\sqrt{1 + \dfrac{m_a^2}{p_a^2}} \approx p_a + \dfrac{m_a^2}{2p_a}$,

with $\mathbf{p_a} \equiv (E_a, \vec{p}_a) = (E_a, p_a, 0, 0)$ the 4–momentum in the vacuum.

2.2.1 Neutrino oscillations in the vacuum

Neutrinos propagating in the vacuum are not affected by external surrounding particles, and hence the probability of oscillation is defined as the square of the amplitude, so

$$\begin{aligned} P_{(\nu_\alpha \to \nu_\beta)}(t) \equiv & |\mathcal{A}_{\nu_\alpha \to \nu_\beta}|^2 \\ = & \sum_{b=1}^{n} U_{\alpha b} U_{\beta b}^* e^{-i\frac{m_b^2}{2E}L} \sum_{a=1}^{n} U_{\alpha a}^* U_{\beta b} e^{-i\frac{m_a^2}{2E}L} \\ = & \sum_{a=1}^{n}\sum_{b=1}^{n} U_{\alpha a}^* U_{\beta a} U_{\alpha b} U_{\beta b}^* e^{i\frac{\Delta m_{ab}^2}{2E}L} \\ = & \sum_{a=1}^{n}\sum_{b=1}^{n} J_{\alpha\beta}^{ab} e^{i\frac{\Delta m_{ab}^2}{2E}L} \ . \end{aligned} \tag{2.10}$$

where $\Delta m_{ab}^2 \equiv m_a^2 - m_b^2$ are the square mass differences and we define $J_{\alpha\beta}^{ab} \equiv U_{\alpha a}^* U_{\beta a} U_{\alpha b} U_{\beta b}^*$ as the amplitude parameter with the following properties:

- $J_{\alpha\beta}^{ab} = \left(J_{\beta\alpha}^{ab}\right)^*$,
- $J_{\alpha\beta}^{ab} = \left(J_{\alpha\beta}^{ba}\right)^*$,
- $\Re\left(J_{\alpha\beta}^{ab}\right) = \Re\left(J_{\beta\alpha}^{ab}\right) = \Re\left(J_{\alpha\beta}^{ba}\right)$,
- $\Im\left(J_{\alpha\beta}^{ab}\right) = -\Im\left(J_{\beta\alpha}^{ab}\right) = -\Im\left(J_{\alpha\beta}^{ba}\right)$.

Taking into account these relations, another way to rewrite Equation (2.10) is

$$P_{\nu_\alpha \to \nu_\beta} \equiv P_{\alpha\beta} = \delta_{\alpha\beta} - 4\sum_{\substack{a=1 \\ a<b}}^{n}\sum_{b=1}^{n} \Re\left(J_{\alpha\beta}^{ab} \sin^2\left(\frac{\Delta m_{ab}^2}{4E}L\right)\right) + 2\sum_{\substack{a=1 \\ a<b}}^{n}\sum_{b=1}^{n} \Im\left(J_{\alpha\beta}^{ab} \sin\left(\frac{\Delta m_{ab}^2}{2E}L\right)\right) \ , \tag{2.11}$$

It is worth mentioning that for antineutrinos, the complex term only changes sign, such that $P_{\bar{\alpha}\bar{\beta}} = P_{\beta\alpha}$.

It is common to express E_ν and m_a in eV or scalar multiples of these units. Thus, Equation (2.11) relates the natural and SI systems of units using a conversion factor of $f = 1.267$, resulting in

$$\frac{\Delta m^2_{ab}}{4E_\nu} \simeq 1.267 \frac{\Delta m^2_{ab}\ (\mathrm{eV})^2\ L(\mathrm{m})}{E_\nu\ (\mathrm{MeV})} \simeq 1.267 \frac{\Delta m^2_{ab}\ (\mathrm{eV})^2\ L(\mathrm{km})}{E_\nu\ (\mathrm{GeV})}\ . \tag{2.12}$$

Likewise, we can assume that neutrino propagation time is proportional to its distance traveled. Then, the oscillation phase is obtained from the sinusoidal terms as $\phi_{kj} = -\Delta m^2_{kj} L/(2E)$ and the oscillation length in the vacuum (typical distance in which the oscillation phase is equal to a 2π period) could be expressed as $L_{\mathsf{osc,v}} = (4\pi E)/\Delta m^2_{kj}$. Thus, in order to have important oscillation effects, this oscillation length must be greater than the distance between source and detector; otherwise, we can only treat average oscillation effects (Jarlskog, 1985).

2.2.2 Neutrino oscillations in matter

Similar to the vacuum case, the Schrödinger equation in the mass eigenstate basis is

$$i\frac{d}{dt}\psi_m(t) = \mathcal{H}_m \psi_m(t), \tag{2.13}$$

where

$$\mathcal{H}_m = H_m + V_m\ ,$$

is the mass Hamiltonian. In the same way, for the flavor eigenstate basis

$$i\frac{d}{dt}\psi_f(t) = \mathcal{H}_f \psi_f(t), \tag{2.14}$$

where

$$\mathcal{H}_f = H_f + V_f.$$

In the mass eigenstate basis, the matter term (the potential matrix) is

$$V_m = U^{-1} V_f U. \tag{2.15}$$

Thus, the total Hamiltonian in the mass eigenstate basis is given by

$$\mathcal{H}_m = H_m + U^{-1} V_f U. \tag{2.16}$$

The solution for the Schrödinger equation (2.13) is given by

$$|\psi_m(t)\rangle = e^{-i\mathcal{H}_m t}\,|\psi_m(0)\rangle\,. \tag{2.17}$$

Substituting $t = L$ into Equation (2.17), we find the solution in the mass basis as

$$\psi_m(L) = e^{-i\mathcal{H}_m L}\psi_m(0) \equiv U_m(L)\psi_m(0)\ , \tag{2.18}$$

and in the flavor state basis

$$\psi_f(L) \;=\; U\psi_m(L) = Ue^{-i\mathcal{H}_m L}\psi_m(0) = Ue^{-i\mathcal{H}_m L}U^{-1}U\psi_m(0) = Ue^{-i\mathcal{H}_m L}U^{-1}\psi_f(0)\ . \tag{2.19}$$

2.2.3 Neutrino potentials in matter

When neutrinos propagate in matter, the three flavors interact through neutral current (NC) weak interactions mediated by the Z^0 boson, with the protons, electrons, and neutrons present in the surrounding ordinary matter, while electrons are the only charged particles capable of interact weakly in charged current (CC) through $W^{\pm}$ bosons (see Figure 2.2). These interactions modify the effective mass of particles as they move. This phenomenon is analogous to the propagation of photons, which have no mass in the vacuum but in a medium acquire an effective mass and, as a result, are unable to travel at the speed of light c within this medium. Because of this effect, neutrino flavor transitions within a medium are invariably different from those present in the vacuum. As a result, an effective potential is added to the Hamiltonian in the Schrödinger Equation.

$$i\frac{d\Psi(t)}{dt} = \mathcal{H}_{\text{eff}}\Psi(t) \ . \tag{2.20}$$

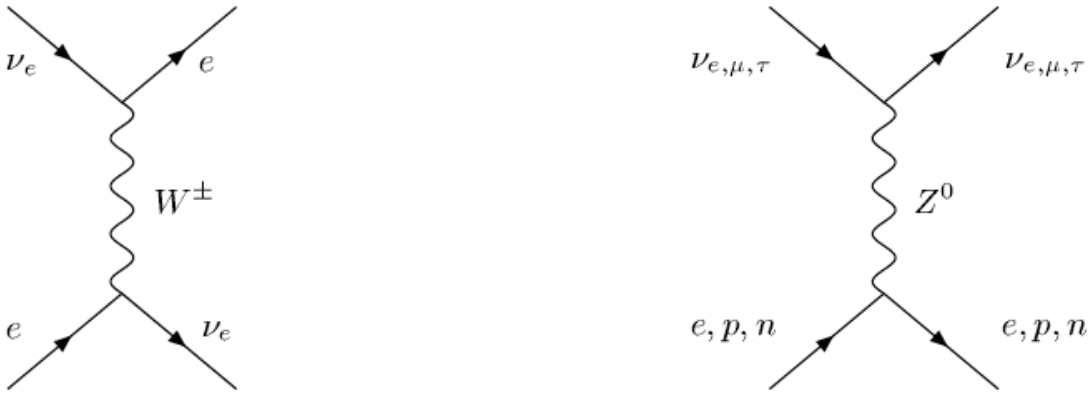

Figure 2.2: *Feynman diagrams of elastic scattering interactions between neutrinos and matter. The CC diagram is on the left, while the NC diagram is on the right.*

The resulting potential will be proportional to the Fermi constant and will incorporate both possible interactions $V_{\text{eff}} = V_{W^{\pm}} + V_{Z^0}$ where

$$V_{W^{\pm}} = \begin{cases} +\sqrt{2}G_F N_e, & \forall\ \nu_e \\ -\sqrt{2}G_F N_e, & \forall\ \bar{\nu_e} \end{cases} \ , \tag{2.21}$$

$$V_{Z^0} = \begin{cases} -\frac{1}{\sqrt{2}}G_F N_n, & \forall\ \nu_x \\ +\frac{1}{\sqrt{2}}G_F N_n, & \forall\ \bar{\nu}_x \end{cases} \ , \tag{2.22}$$

with $x = e, \mu, \tau$ and $N_e = Y_e\rho/m_N$; (N_n) is the electron (neutron) number density.

Therefore, by incorporating both interactions, the effective Hamiltonian within a medium is

$$\mathcal{H}_{\text{eff}} = UH_{\text{vac}}U^{-1} + V_m \ , \tag{2.23}$$

where the potential term is expressed as

$$V_m = \begin{pmatrix} V_e & 0 & 0 \\ 0 & V_\mu & 0 \\ 0 & 0 & V_\tau \end{pmatrix} = \begin{pmatrix} V_{\rm CC} + V_{\rm NC} & 0 & 0 \\ 0 & V_{\rm NC} & 0 \\ 0 & 0 & V_{\rm NC} \end{pmatrix} , \tag{2.24}$$

where $V_{\rm CC} \equiv V_{W^\pm}$ and $V_{\rm NC} \equiv V_{Z^0}$. The Equation (2.21) is usually expressed in terms of more convenient units as follows

$$V_{\rm CC} \simeq 7.54 \times 10^{-14} \;\; Y_e \; \frac{\rho}{\rm g \; cm^{-3}} \; {\rm eV} \; . \tag{2.25}$$

It is worth nothing that the Hamiltonian in flavor basis is used when neutrinos propagate through vacuum $H_f = UH_mU^{-1}$, where the representation of H_f in an exponential form is given by, $U_f(t) = e^{-iH_f t} = Ue^{-iH_m t}U^{-1}$. When neutrinos travel through matter, however, the Hamiltonian is not diagonal neither in the mass nor in the flavor eigenstate basis, and we must compute numerically the operator $U_f(t)$ for every particular case.

It is important to note here that since all NC entries of the Equation (2.24) are equal, the contributions will be the same for all flavors of neutrinos. Furthermore, if the medium in which these particles propagate tends to be electrically neutral $(Y_e \simeq 0.5)$, then approximately the same amount of neutrons and protons are expected, such that $N_e = N_n$, and thus these NC contributions would also cancel each other out. As a result, all the diagonal terms of V_m will only affect the phase of the evolution operator and therefore have no effect on the oscillation probabilities. In other words, we can ignore the NC contribution throughout this study.

2.2.4 Neutrino potentials in matter with a magnetic contribution

In order to incorporate the magnetic field contributions into the neutrino scattering relations it is necessary to use finite temperature quantum field theory, which is typified by the usage of the medium's contributions to the real and imaginary parts of the neutrino scattering function (Tututi et al., 2002) within the Schwinger time frame (Schwinger, 1951). This requires the introduction of a new term, which we call neutrino self-energy, and it is represented by the variable $\Sigma \equiv \Sigma_W + \Sigma_Z + \Sigma_t$. These interactions can be reconstructed graphically using different self-energy diagrams expressed as a combination of one-loop interactions with weak interaction mediator particles ($W^\pm$ and Z^0 bosons) existing in the medium in which it propagates (see Figure 2.3).

In this section we will describe the effective potentials of the neutrino immersed in media with different magnetic fields, for simplicity we will call them strong, mild and weak, concerning the Landau's critical magnetic field of the electrons defined as $B_c = m_e c^2/2\mu_e = m_e^2 c^3/e\hbar \sim 4.414 \times 10^{13}$ G and represented as the dimensionless parameter of the magnetic field $\Omega_B \equiv B/B_c$.[5]

[5] An explicit derivation for these limit cases can be found in Fraija (2014).

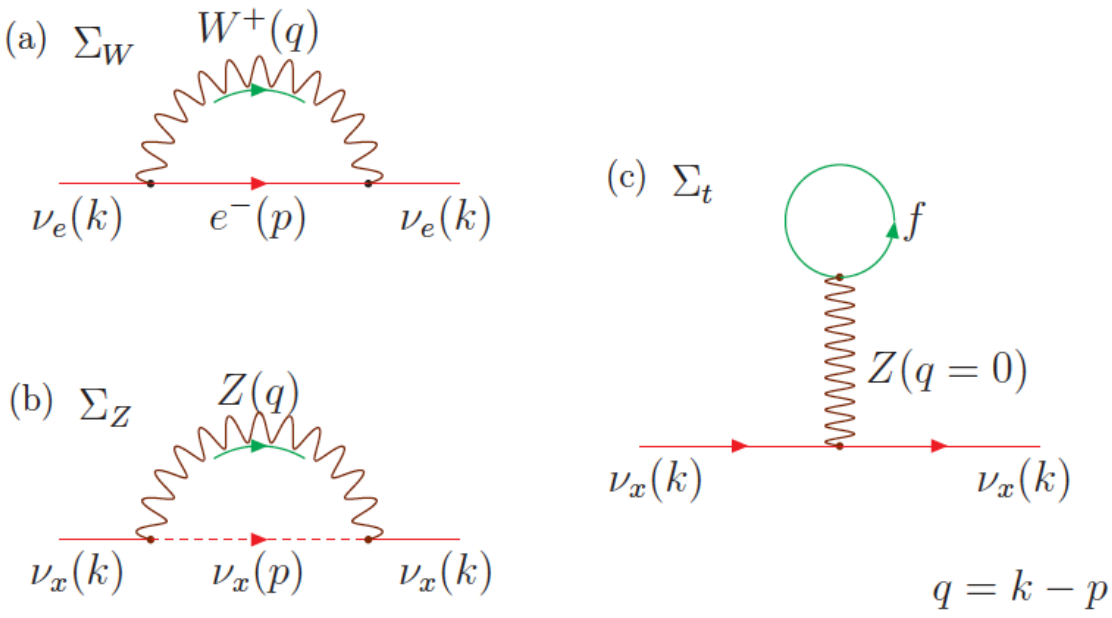

Figure 2.3: *Contribution of a single loop to the neutrino self-energy in a magnetic medium. (a) $W-$exchange diagram: the solid line represents the electron propagator, while the wavy line represents the W boson in a magnetized medium. (b) $Z-$exchange diagram: the dashed line represents the neutrino propagator in a thermal medium, and the wiggly line represents the Z boson. (c) Tadpole diagram: the solid line represents the fermion propagator, while the wavy line represents the Z boson in a magnetic medium. This figure is taken from Fraija (2014).*

Strong magnetic field $(\Omega_B > 1)$

In a medium with a strong magnetic field $(\Omega_B \equiv eB/m_e^2 \gg 1)$, all leptons are confined to the Landau zero level $(\lambda_n^2 = 0)$ and therefore, the electron energy is $E_{e,0}^2 = (p_3^2 + m_e^2)$, so the potential acquire the form

$$
\begin{aligned}
V_{\text{eff,S}} = \quad & \frac{\sqrt{2} G_F\, m_e^3}{\pi^2} \Omega_B \left[\sum_{l=0}^{\infty} (-1)^l \sinh \alpha_l \, K_1(\sigma_l) \right. \\
& \times \left\{ 1 + \frac{m_e^2}{m_W^2} \left(\frac{3}{2} + 2\frac{E_\nu^2}{m_e^2} + \Omega_B \right) \right. \\
& \left. \left. - \left(1 + \frac{m_e^2}{m_W^2} \left(\frac{1}{2} - 2\frac{E_\nu^2}{m_e^2} + \Omega_B \right) \right) \cos\phi \right\} \right. \\
& - 4 \frac{m_e^2}{m_W^2} \frac{E_\nu}{m_e} \sum_{l=0}^{\infty} (-1)^l \cosh \alpha_l \\
& \left. \times \left\{ \frac{3}{4} K_0(\sigma_l) + \frac{K_1(\sigma_l)}{\sigma_l} - \frac{K_1(\sigma_l)}{\sigma_l} \cos\phi \right\} \right] ,
\end{aligned}
\tag{2.26}
$$

where m_W is the mass of boson W, K_n is the modified Bessel function of order n. Temperature

($T = \beta^{-1}$) and chemical potential (μ) are incorporated through the following relations

$$\alpha_l = \beta\mu(l+1), \quad \sigma_l = \beta m_e(l+1)\ . \tag{2.27}$$

Mild magnetic field $\Omega_{\mathbf{B}} \simeq \mathbf{1}$

Considering a moderate magnetic field of order B_c, charged leptons begin to populate the upper Landau levels, so the contributions of these levels to the effective potential now become important.

$$\begin{aligned} V_{\text{eff,M}} = \quad & \frac{\sqrt{2}G_F\, m_e^3}{\pi^2}\Omega_B\left[\sum_{l=0}^{\infty}(-1)^l \sinh\alpha_l \left\{\frac{m_e^2}{m_W^2}\left(1+4\frac{E_\nu^2}{m_e^2}\right)K_1(\sigma_l)\right.\right. \\ & \left.+\sum_{n=1}^{\infty}\lambda_n\left(2+\frac{m_e^2}{m_W^2}\left(3-2\Omega_B+4\frac{E_\nu^2}{m_e^2}\right)\right)K_1(\sigma_l\lambda_n)\right\} \\ & -4\frac{m_e^2}{m_W^2}\frac{E_\nu}{m_e}\sum_{l=0}^{\infty}(-1)^l\cosh\alpha_l\left\{\frac{3}{4}K_0(\sigma_l)\right. \\ & \left.\left.+\sum_{n=1}^{\infty}\lambda_n^2\,K_0(\sigma_l\lambda_n)\right\}\right], \end{aligned} \tag{2.28}$$

with $A_e = \sqrt{2}G_F\left(\frac{m_e^3\,\Omega_B}{\pi^2}\right)$ and

$$\lambda_n^2 = \begin{cases} 2n\Omega_B & \text{for } \Omega_B > 1 \\ 1+2n\Omega_B & \text{for } \Omega_B \leq 1\,. \end{cases}$$

Weak magnetic field $\Omega_{\mathbf{B}} < \mathbf{1}$

Considering a weak magnetic field ($eB \ll m_e^2$), charged leptons now occupy all Landau levels and it is possible to assume that they contribute continuously to the sums (i.e. $\sum_n \to \int dn$) of $\lambda = \sqrt{1+2n\,\Omega_B}$. Under this assumption the effective potential results in

$$\begin{aligned} V_{\text{eff,W}} = \quad & \frac{\sqrt{2}G_F\, m_e^3}{\pi^2}\Omega_B\left[\sum_{l=0}^{\infty}(-1)^l\sinh\alpha_l\left\{\left(2+\frac{m_e^2}{m_W^2}\left(3+4\frac{E_\nu^2}{m_e^2}\right)\right)\right.\right. \\ & \left.\times\left(\frac{K_0(\sigma_l)}{\sigma_l}+2\frac{K_1(\sigma_l)}{\sigma_l^2}\right)\Omega_B^{-1}-2\left(1+\frac{m_e^2}{m_W^2}\right)K_1(\sigma_l)\right\} \\ & -4\frac{m_e^2}{m_W^2}\frac{E_\nu}{m_e}\sum_{l=0}^{\infty}(-1)^l\cosh\alpha_l\left\{\left(\frac{2}{\sigma_l^2\,\Omega_B}-\frac{1}{4}\right)K_0(\sigma_l)\right. \\ & \left.\left.+\left(1+\frac{4}{\sigma_l^2}\right)\frac{K_1(\sigma_l)}{\sigma_l}\Omega_B^{-1}\right\}\right]. \end{aligned} \tag{2.29}$$

2.2.5 Oscillation probabilities within a medium of constant density

An examination of Equation (2.13) in the context of a medium of constant density revealed that the conversion probabilities between flavors are given by Gonzalez-Garcia & Nir (2003)

$$\begin{aligned}
P_{ee} &= 1 - 4s^2_{13,m}c^2_{13,m}S_{31}\,,\\
P_{\mu\mu} &= 1 - 4s^2_{13,m}c^2_{13,m}s^4_{23}S_{31} - 4s^2_{13,m}s^2_{23}c^2_{23}S_{21} - 4c^2_{13,m}s^2_{23}c^2_{23}S_{32}\,,\\
P_{\tau\tau} &= 1 - 4s^2_{13,m}c^2_{13,m}c^4_{23}S_{31} - 4s^2_{13,m}s^2_{23}c^2_{23}S_{21} - 4c^2_{13,m}s^2_{23}c^2_{23}S_{32}\,,\\
P_{e\mu} &= 4s^2_{13,m}c^2_{13,m}s^2_{23}S_{31}\,,\\
P_{e\tau} &= 4s^2_{13,m}c^2_{13,m}c^2_{23}S_{31}\,,\\
P_{\mu\tau} &= -4s^2_{13,m}c^2_{13,m}s^2_{23}c^2_{23}S_{31} + 4s^2_{13,m}s^2_{23}c^2_{23}S_{21} + 4c^2_{13,m}s^2_{23}c^2_{23}S_{32}\,,
\end{aligned} \tag{2.30}$$

where $\theta_{13,m}$ is the effective mixing angle in matter

$$\sin 2\theta_{13,m} = \frac{\sin 2\theta_{13}}{\sqrt{\left(\cos 2\theta_{13} - \frac{2E_\nu V_{\text{eff}}}{\Delta m^2_{32}}\right)^2 + (\sin 2\theta_{13})^2}}\,, \tag{2.31}$$

and S_{ij}, denotes the oscillation factors in matter defined as

$$S_{ij} = \sin^2\left(\frac{\Delta\mu^2_{ij}L}{4E_\nu}\right). \tag{2.32}$$

with $\Delta\mu^2_{ij}$ the difference of effective masses in matter where the following relations are fullfilled:

$$\begin{aligned}
\Delta\mu^2_{21} &= \frac{\Delta m^2_{32}}{2}\left(\frac{\sin 2\theta_{13}}{\sin 2\theta_{13,m}} - 1\right) - E_\nu V_{\text{eff}}\,,\\
\Delta\mu^2_{32} &= \frac{\Delta m^2_{32}}{2}\left(\frac{\sin 2\theta_{13}}{\sin 2\theta_{13,m}} + 1\right) + E_\nu V_{\text{eff}}\,,\\
\Delta\mu^2_{31} &= \Delta m^2_{32}\left(\frac{\sin 2\theta_{13}}{\sin 2\theta_{13,m}}\right),
\end{aligned} \tag{2.33}$$

with the sine and cosine functions defined as

$$\begin{aligned}
\sin 2\theta_{13,m} &= \frac{1}{2}\left(1 - \sqrt{1 - \sin 2\theta_{13,m}}\right),\\
\cos 2\theta_{13,m} &= \frac{1}{2}\left(1 + \sqrt{1 - \sin 2\theta_{13,m}}\right).
\end{aligned} \tag{2.34}$$

In this context, the oscillation length in matter is given by

$$L_{\text{osc,mat}} = \frac{L^{\text{osc}}_0}{\sqrt{\cos^2 2\theta_{13}(1 - \frac{2E_\nu V_{\text{eff}}}{\Delta m^2_{32}\cos 2\theta_{13}})^2 + \sin^2 2\theta_{13}}}\,, \tag{2.35}$$

with $L^0_{\text{osc}} = \dfrac{4\pi E_\nu}{\Delta m^2_{32}}$, the length of oscillation in vacuum, where it is required that

$$\cos 2\theta_{13} = \frac{2E_\nu V_{\text{eff}}}{\Delta m^2_{32}}\,, \tag{2.36}$$

to satisfy the resonance condition. Thus, the resonance length is determined by means of

$$L_{\text{res}} = \frac{L^0_{\text{osc}}}{\sin 2\theta_{13}}\,. \tag{2.37}$$

Until now, it has been assumed that V_{eff} does not fluctuate with distance; nevertheless, these effects must be considered by introducing the adiabatic condition into this process. This criterion is met in this scenario when (Fraija, 2010)

$$\kappa_{\text{res}} \equiv \frac{2}{\pi}\left(\frac{\Delta m^2_{32}}{2E_\nu}\sin 2\theta_{13}\right)^2\left(\frac{dV_{\text{eff}}}{dr}\right)^{-1} \geq 1\,, \tag{2.38}$$

with $r = lx$ and x adimensional.

2.2.6 Medium with a variable density

In a medium with a variable density, the neutrino properties are modified and governed primarily by an adiabaticity condition. The concept of adiabaticity is related to how quickly the system adapts to changing external conditions. In the ideal case, we demand a smooth change in the baryonic density. If the density varies smoothly as a function of distance, the neutrino states' changes can be negligible. Therefore, the flavor admixtures are preserved and can take representative values of the density.

Adiabaticity parameter and flip probability

The dynamics of the transitions are determined by the adiabaticity parameter (Parke, 1986; Dighe & Smirnov, 2000)

$$\gamma_{\text{ad}} \equiv \frac{\Delta m^2}{2E_\nu}\frac{\sin^2 2\theta}{\cos 2\theta}\frac{1}{\frac{1}{n_e}\frac{dn_e}{dr}}\,, \tag{2.39}$$

and the probability that a defined neutrino in a mass eigenstate jumps to another, the so-called flip probability is defined as

$$P_f = e^{-\frac{\pi\gamma_{\text{ad}}}{2}}\,, \tag{2.40}$$

which is given by the linear approximation of the Landau-Zener formula. In this context, the adiabaticity condition is satisfied when $\gamma_{\text{ad}} \gg 1$, at all locations along the path, the evolution is considered to be adiabatic, and the off-diagonal Hamiltonian components can be ignored. Furthermore, this parameter can be expressed as a function of a power-law density profile $\rho = Ar^{-n}$ as follows

$$\gamma_{\text{ad}} = \frac{1}{2n}\left(\frac{\Delta m^2}{E_\nu}^{1-\frac{1}{n}}\right)\frac{\sin^2 2\theta}{(\cos 2\theta)^{1+\frac{1}{n}}}\left(\frac{2\sqrt{2}G_F Y_e}{m_N}A\right)^{\frac{1}{n}}\,, \tag{2.41}$$

where the resonance condition has been used to indicate the distance contribution through the oscillation parameters, and the number density of electrons was expressed as $N_e = Y_e\rho(r)/m_N$.

Resonance energies

It is observed that under the resonance condition, there are two key energies that correspond to the maximum value of the electron density within the medium. These resonance energies are defined as

$$E^L_{\rm res} \approx \frac{\Delta m^2_{21}}{2V_{\rm eff}} \cos 2\theta_{12} \ ; \qquad E^H_{\rm res} \approx \frac{\Delta m^2_{31}}{2V_{\rm eff}} \cos 2\theta_{13} \ . \tag{2.42}$$

Both energies delimit three regions of interest where different flavor conversion dynamics dominate, as a result of the Hamiltonian's contribution. $E_\nu < E^L_{\rm res}$ depicts the vacuum transition domain, whereas $E^L_{\rm res} < E_\nu < E^H_{\rm res}$ denotes the area influenced by matter effects but still within the adiabatic regime. Finally, $E^H_{\rm res} \ll E_\nu$ represents the region in which neutrino oscillations are suppressed within matter, and it is preferable to adopt an approximation as an average of the oscillations caused by a loss of coherence.

2.2.7 Three-flavor oscillation parameters

Table (2.1) summarizes the most up-to-date measurement of the oscillation parameters in the three-flavor mixture obtained from a global analysis. The acquisition of these parameters themselves is a milestone in modern experimental physics and retrieves a large collection of data from multiple experiments to provide accurate measurements. To learn in detail the physics behind each measurement, the reader is suggested to review de Salas et al. (2021).

2.2.8 Neutrino parametrization

Because terrestrial detectors cannot measure oscillation probabilities, they must rely on physically quantifiable variables. So the probability matrix must be expressed in terms of the expected neutrino flavor ratio. This is accomplished by incorporating the neutrino flux before and after oscillations take place: $\Phi = P_{\alpha\beta}\ \Phi^0$, where $P_{\alpha\beta}$ denotes the probability matrix between the initial $\Phi^0 = (\Phi^0_e, \Phi^0_\mu, \Phi^0_\tau)$ and final $\Phi = (\Phi_e, \Phi_\mu, \Phi_\tau)$ neutrino fluxes. Although there are many ways to do this, for simplicity, we will use the parameterization proposed by Palladino & Vissani (2015).

$$\xi_n = \Phi / \sum_n \Phi_n \ , \tag{2.43}$$

where ξ is defined as the fraction of neutrinos with a defined flavor. Thus, if the initial neutrino fraction $(\xi_e, \xi_\mu, \xi_\tau)_0 \equiv (f, g, h)$ is known, the neutrino rate after propagation can be parametrized as

$$\xi_e = \frac{1}{3} + (2 - 3g - 3h)P_0 + (g - h)P_1 \ ,$$

Parameter	Best-fit $\pm1\sigma$ (NO)	Best-fit $\pm1\sigma$ (IO)
$\sin^2\theta_{12}$	$0.310^{+0.013}_{-0.012}$	$0.310^{+0.013}_{-0.012}$
$\theta_{12}/\ (^\circ)$	$33.82^{+0.78}_{-0.76}$	$33.82^{+0.78}_{-0.75}$
$\sin^2\theta_{23}$	$0.582^{+0.015}_{-0.019}$	$0.582^{+0.015}_{-0.018}$
$\theta_{23}/\ (^\circ)$	$49.7^{+0.9}_{-1.1}$	$49.7^{+0.9}_{-1.0}$
$\sin^2\theta_{13}$	$0.02240^{+0.00065}_{-0.00066}$	$0.02263^{+0.00065}_{-0.00066}$
$\theta_{13}/\ (^\circ)$	$8.61^{+0.12}_{-0.13}$	$8.65^{+0.12}_{-0.13}$
$\frac{\Delta m^2_{21}}{10^{-5}\ \text{eV}^2}$	$7.39^{+0.21}_{-0.20}$	$7.39^{+0.21}_{-0.20}$
$\frac{\Delta m^2_{31}}{10^{-3}\ \text{eV}^2}$	$2.525^{+0.033}_{-0.031}$	$-2.512^{+0.034}_{-0.031}$

Table 2.1: *We show the best-fit parameters for a three-flavor mixing scenario under a Normal Ordering (NO) scheme ($\Delta m^2_{31} > 0$; left column) and an Inverted Ordering (IO) scheme ($\Delta m^2_{31} < 0$; right column). These parameters were derived within $\pm1\sigma$ range from global data analysis (de Salas et al., 2021).*

$$\begin{aligned}\xi_\mu =&\frac{1}{3}+\frac{1}{2}(-2+3g+3h)P_0+(1-2g-h)P_1+(g-h)P_2\ ,\\ \xi_\tau =&\frac{1}{3}+\frac{1}{2}(-2+3g+3h)P_0+(-1+g+2h)P_1-(g-h)P_2\ ,\end{aligned} \tag{2.44}$$

here P_0 P_1 and P_2 is expressed in terms of the probabilities as follows:

$$\begin{aligned}P_0 =&\frac{P_{ee}-\frac{1}{3}}{2}\ ,\\ P_1 =&\frac{P_{e\mu}-P_{e\tau}}{2}\ ,\\ P_2 =&\frac{P_{\mu\mu}+P_{\tau\tau}-2P_{\mu\tau}}{4}\ .\end{aligned} \tag{2.45}$$

2.3 Neutrino detection

In order to detect neutrinos, we can study their weak interactions when they move through a non-empty medium. For example, when neutrinos interact with particles in a medium like water, they produce charged leptons that travel at superluminal speeds, resulting in an energetic cone-shaped flash akin to a plane breaking the sound barrier. Čerenkov radiation is the name for this phenomenon and is the foundation for sizeable water-based neutrino detectors. However, in order to increase the likelihood of these particles being detected, they must meet the

following criteria: i) a broad detection cross-section, ii) a large mass (upper the kiloton scale), iii) a remarkable energy resolution (to identify and explore the predicted energy window), and iv) a strong signal discrimination over background noise.

These neutrinos are detected primarily by observing the muon traces produced by interactions with nucleons. In particular, reactions of type $(\nu_l, \bar{\nu}_l) \rightarrow (l^-, l^+)$ and $(\nu_l, \bar{\nu}_l)N \rightarrow (\nu_l, \bar{\nu}_l)$ are the major source of these signals. In this context, large underground Čerenkov detectors are becoming increasingly important. Typically, each detector is surrounded by an array of photomultipliers (PMT) that allow the weak incident signal produced by the photons to be amplified by several orders of magnitude. By observing these photons and knowing the arrival time at each PMT, the trajectory, direction and energy of the original trace can be reconstructed. Some of the most important detectors to consider are described below.

2.3.1 Neutrino detectors

Super-Kamiokande

In a Japanese mine, a neutrino observatory known as Super-Kamiokande (Super–K) was installed 1000 meters underground to study neutrinos. Super–K is a gigantic water Čerenkov detector with a base 39 meters in diameter and a height of 42 meters, and it has the ability to hold 50 kton of ultra-pure water. Super–K contains a photomultiplier (PMT) array with almost 13,000 sensors divided into two sections: 11,129 PMT within the inner region and 1,885 PMT in the outer region. Research in the MeV energy range is carried out by the Super–K outreach in the areas of solar neutrinos, accelerator neutrinos, and atmospheric neutrinos, as well as proton decay (Fukuda et al., 2003; Beacom & Vagins, 2004; Suzuki, 2019; Abe et al., 2022).

Hyper−Kamiokande

After a successful first phase in the construction of Čerenkov water detectors on the kiloton scale, the technology is venturing into the next step by constructing more giant detectors on the megaton scale. Proof of this is the future Hyper-Kamiokande (Hyper-K) modular neutrino detector. Modularity would result in a lower volume (for equivalent total mass) than a single tank. However, it is appealing since it divides various problems (excavation, instrumentation, maintenance) into more manageable parts that may be done progressively. The modular architecture significantly reduces waiting time since it may begin delivering data as soon as the first module is ready, as was the case with the IceCube detector (Lunardini, 2016).

Following the principles of its predecessor, Hyper-K will be a subway detector surrounded by a thick layer of rock that will serve as a veto to block the cascade of surface particles that are produced by cosmic rays and other background radiation. It will be dug in two new cylindrical-shaped caverns in the Tochibora mine, about 8 kilometers south of Super-K, and is expected to be operational by 2027. It will have a fiducial mass of 0.56 million metric tons. The basic design of Hyper-K will have 99,000 newly designed high-efficiency and high-resolution PMTs, making it the world's biggest subterranean water Čherenkov detector. The detector will be filled with clear, ultra-pure water, with an anticipated light attenuation length of more than

100 meters. Its main objective will be to perform more precise measurements of the oscillation parameters in neutrinos as well as the study of Charge-Parity (CP) violation in the leptonic sector. (Abe et al., 2011, 2018a,b; Kudenko, 2020).

DUNE

The DUNE experiment (*Deep Underground Neutrino Experiment*) will consist of a detector composed of a 40 kton fiducial mass of Liquid Argon attached to the science facilities of the LBNF experiment (*Long–Baseline Neutrino Facility*), located in South Dakota, USA. Liquid argon is particularly sensitive to interaction by charged currents of the ν_e component from the incident neutrino flux. Therefore, measurements are made primarily by neutron absorption in $^{40}\mathrm{Ar}$, generating an excited $^{40}\mathrm{K}^*$ nucleus and an electron ($\nu_e + ^{40}\mathrm{Ar} \rightarrow ^{40}\mathrm{K}^* + e^-$). In a further de-excitation process, this $^{40}\mathrm{K}^*$ emits a cascade of photons. The detector measures the combined mixture of these electrons and photons as short pulses in the MeV energy range (De Gouvêa et al., 2020).

It is expected to start operating by 2026. Its main objectives include searching for proton decay, measurements of neutrino parameters produced in particle accelerators, and detecting astrophysical neutrinos. In particular, DUNE will be able to detect neutrinos from transient events such as SNe and GRB, measuring critical information for the understanding of the dynamics of these events (Adams et al., 2013; Goodman, 2015; Lunardini, 2016; Acciarri et al., 2016).

2.3.2 Number of neutrino expected events

The number of events in a neutrino detector can be estimated as

$$N_{\mathrm{ev}} = N_T \int_{t_i}^{t_f} \int_{E_{\mathrm{min}}}^{E_{\mathrm{max}}} \Phi(E,t)\sigma(E) dE dt \ , \tag{2.46}$$

where N_T represents the number of target protons in the detector, E is the neutrino energy, $\Phi(E,t)$ is the number flux of neutrinos per unit energy and $\sigma(E)$ is the capture cross-section. This expression can be expressed in an analogous way as

$$N_{\mathrm{ev}} = V_{\mathrm{det}} N_A \, \rho_N \int_{t'} \int_{E'} \sigma_{cc}^{\bar{\nu}_e p}(E) \frac{dN}{dE} \, dE dt \, , \tag{2.47}$$

where V_{det} is the effective volumen of water, $N_A = 6.022 \times 10^{23}$ g^{-1} is the Avogadro's number, $\rho_N = (M_{\mathrm{fiducial}}/V_{\mathrm{det}}) = 2/18\,\mathrm{g\,cm^{-3}}$ is the nucleons density in water, $\sigma_{cc}^{\bar{\nu}_e p} \simeq 9 \times 10^{-44}\, E^2_{\bar{\nu}_e}/\mathrm{MeV}^2$ is the neutrino cross-section (Bahcall, 1989), dt is the neutrino emission time and dN/dE is the neutrino spectrum, so the number of events can be approximated as

$$N_{\mathrm{ev}} \simeq \frac{N_A \rho_N \sigma_{CC}^{\bar{\nu}_e p}}{4\pi d_z^2 \, \langle E_{\bar{\nu}_e} \rangle} V_{\mathrm{det}} \ E_{T,\bar{\nu}_e} \, , \tag{2.48}$$

where d_z is the distance from neutrino production to Earth, $\langle E_{\bar{\nu}_e} \rangle$ is the average energy of electron antineutrino and $E_{T,\bar{\nu}_e} = \int L_{\bar{\nu}_e} dt$ is the total neutrino energy emitted (Mohapatra

& Pal, 2004; Fraija et al., 2014). For this equation, we have chosen this particular flavor since water Čerenkov neutrino detectors are primarily more sensitive to electron antineutrinos, which are observed via protons' absorption $(\bar{\nu}_e + p \rightarrow e^+ + n)$ (Bahcall, 1989). This, coupled with the fact that the absorption cross-sections are significantly larger (surpassing by at least one order of magnitude all other channels) than those calculated by nucleon scattering in this energy range (Koers & Wijers, 2005; Lunardini, 2016), means that detecting particles of the complementary flavors (mu and tau) contributes only slightly ($\lesssim 4\%$) by scattering in the water and liquid-argon experiments.

The relation $L_\nu = 4\pi d_z^2 F_\nu \langle E \rangle_\nu = 4\pi d_z^2 F_\nu E_\nu^2 (dN/dE_\nu)$ was taken into account and we have considered that neutrino flux luminosity is correlated with the total photon flux as (Halzen, 2007)

$$\int \frac{dN_\nu}{dE_\nu} E_\nu dE_\nu \propto \int \frac{dN_\gamma}{dE_\gamma} E_\gamma dE_\gamma \ , \tag{2.49}$$

some authors even suggest that a large total amount of the energy released during these events is emitted in the form of neutrinos with the proportion $L_\nu = 10^2 L_\gamma$ during the prompt emission (Halzen, 2007; Becker, 2008).

3

Gamma-Ray Bursts and other astrophysical sources

3.1 A brief history of GRB

The discovery of these highly energetic events occurred almost by accident during the Cold War. The development of defense mechanisms between the two belligerents led to the construction of ultra-energetic detectors to prepare for a possible nuclear attack; in particular, the United States developed a project exclusively in charge of detecting explosions and nuclear weapons tests anywhere on Earth. The objective of this project was to find the gamma radiation emitted by these explosions, which is very difficult to mask. Thus, the Vela Space Program was born, consisting of six pairs of detector satellites that were put into orbit between 1964 and 1970 (Bloom, 2011; Berger, 2014).

For a couple of years, most of the activity detected by these satellites came from charged particles generated in the atmosphere by the action of cosmic rays and lightning originating on Earth. However, on July 2, 1967, four Vela satellites detected unusual gamma radiation that did not come from any known terrestrial source or any other object within the Solar System. In the beginning, nobody knew how they were produced or where they came from; in fact, it took almost five years to make them known because they were classified for military reasons. To identify each of these bursts, they were assigned the prefix "GRB", followed by six numbers corresponding to the date they were found.

Since that date, several satellites have been put into operation to study the behavior of GRB. One of them was the CGRO (Compton Gamma Ray Observatory) satellite, which contained the BATSE (Burst and Transient Source Experiment) detector and whose main contribution was to determine for the first time that GRB did not have a preferential distribution along the galactic plane but were isotropic distributed in the Universe, implying that they were originated at extragalactic distances (see Fig. 3.1) (Meegan et al., 1992). The discovery that GRB were isotropically spread across the sky compelled astronomers to look for mechanisms capable of producing the enormous energies required for an extragalactic origin.

The Beppo-SAX satellite captured the first high-resolution picture of a GRB's afterglow in 1997, allowing for the first time to locate a GRB with a great accuracy. Follow-up observa-

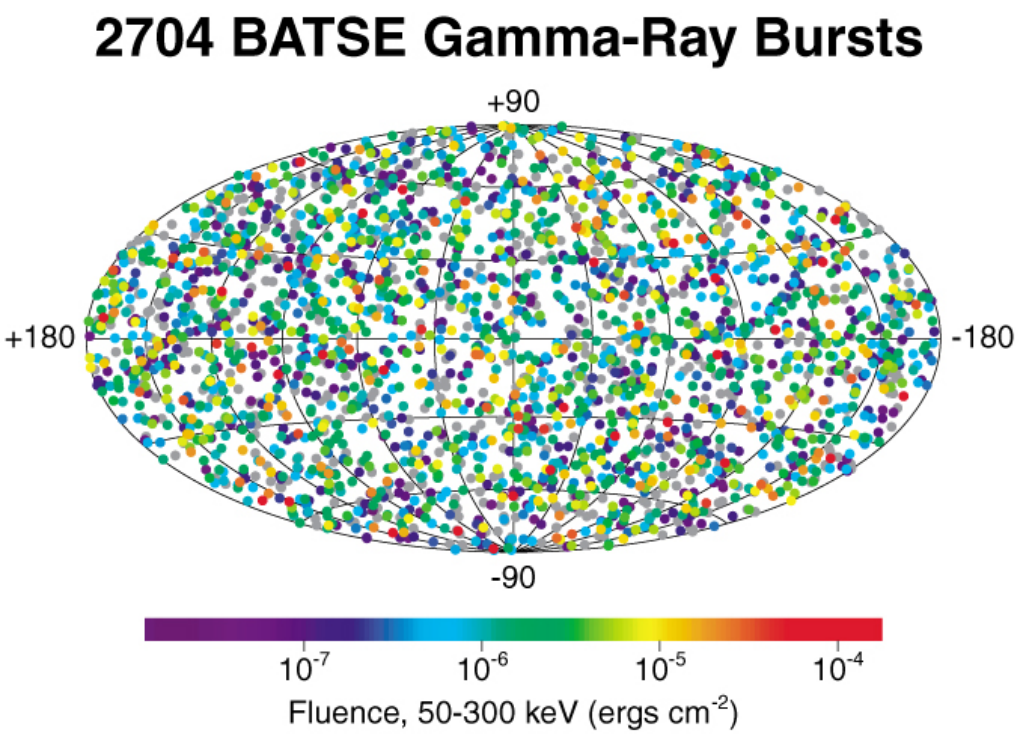

Figure 3.1: *Several GRB observed by BATSE and depicted on galactic coordinates. Bursts are distributed isotropically, regardless of brightness, duration, spectrum, or any other property. It is important to note that there is no preferred galactic or extragalactic direction in this plot, suggesting an extragalactic origin. The colored bar denotes the GRB fluence scale. This figure is taken from Hartmann (1999).*

tions at optical and lower frequencies were possible, resulting in redshift estimates and potential host galaxies. GRB extragalactic origin was confirmed, and a link was discovered between a subgroup of GRB (the so-called Long-soft GRB) and galaxies' star-forming areas, implying a stellar origin (Costa et al., 1997).

The recent *Swift* mission was launched in November 2004. The BAT sensor on *Swift* has not only produced multiple detections, but it has also delivered the first early-time GRB afterglows thanks to its quick response. Before *Swift*, afterglow observations were generally delayed several hours after the burst. However, *Swift*'s ability to identify and then slew to a burst meant that afterglow observations with its BAT instrument could be completed in seconds sensitive to energies between 15 and 150 keV (Barthelmy et al., 2005; Kann et al., 2010; Krimm et al., 2013). Finally, the most recent *Fermi* telescope was launched in June 2008, being sensitive to energies between 10 keV and 25 MeV. The Large Area Telescope (LAT) is its primary instrument (Ackermann et al., 2013a,b). The Gamma-ray Burst Monitor (GBM) is another instrument aboard Fermi that studies GRB and solar flares (Goldstein et al., 2012, 2017).

3.2 The birth of a GRB: Progenitors

Although there are several methods for converting energy, after matter-antimatter annihilation, gravitational energy results the most efficient one. However, since gravitational energy is the weakest fundamental force, it requires a supermassive source for its effects to be significant. Exotic objects capable of a large gravitational potential include very massive compact objects such as black holes, massive stars, and neutron stars.

We now know that the duration of these events varies from a few milliseconds (Fishman et al., 1993) to several minutes (Klebesadel et al., 1984). During this brief time, a large amount of energy is released, between $10^{51} - 10^{54}$ ergs if isotropic emission is assumed, making it the most energetic electromagnetic phenomenon in the Universe (Piran, 1999). This energy is released in a compact region of space of only $\sim 10^{7}$ cm. It is during this process that an opaque "fireball" of gas composed primarily of photons and leptons is generated by the creation of electron-positron pairs (Meszaros & Rees, 1993; Waxman, 1997; Piran, 1999). In these particular conditions, a relativistic collimated jet is produced from the energy extracted from the rotating black hole by the Blandford-Znajek process (Blandford & Znajek, 1977a), through neutrino and antineutrino annihilations or by various magnetohydrodynamic (MHD) processes (Meier et al., 2001; Rosswog & Ramirez-Ruiz, 2002a).

During several years of observation, GRB were found to exhibit a bimodal distribution This bimodality suggests the existence of two distinct classes of progenitors (see Fig. 3.2). On the one hand, the progenitors of LGRB are associated with the collapse of an Ic-type supernova, based on the exclusive location in galaxies with active star formation and by a strong correlation with UV-bright regions in their host galaxies (Woosley, 1993a; Paczyński, 1998; MacFadyen & Woosley, 1999). However, in the case of sGRB, short timescales (on the order of milliseconds) suggest a model of a progenitor based on the merger of two compact objects, such as NS-NS or BH-NS (Eichler et al., 1989; Kochanek & Piran, 1993; Grindlay et al., 2006; Lee & Ramirez-Ruiz, 2007; Faber & Rasio, 2012).

It was initially postulated that the progenitor of these events corresponded to the merger of a binary system, assuming that producing a large amount of energy during a short period had to involve compact objects. (Lattimer & Schramm, 1976; Mészáros, 2000; Eichler et al., 1989), such as that produced by the coalescence of a neutron star-black hole (NS−BH) or a binary neutron star system (NS−NS). (Metzger et al., 2010; Chevalier & Li, 1999) or for the core-collapse of a very massive star (Woosley, 1993a; Paczyński, 1998; MacFadyen & Woosley, 1999). It was until August 17, 2017, that the first model was confirmed when, at 12:41: 04 coordinated universal time (UTC), the LIGO/Virgo collaboration detectors made the first detection in gravitational waves (GW) and a couple of seconds later space and ground-based telescopes recorded at different wavelengths the coalescence of two neutron stars (Abbott et al., 2017). Incredibly the signal recorded by these detectors corresponded to that produced by the merger of these compact objects. In addition, by observing the electromagnetic counterpart associated with this event, it was finally confirmed that this is the mechanism through which an sGRB is produced.

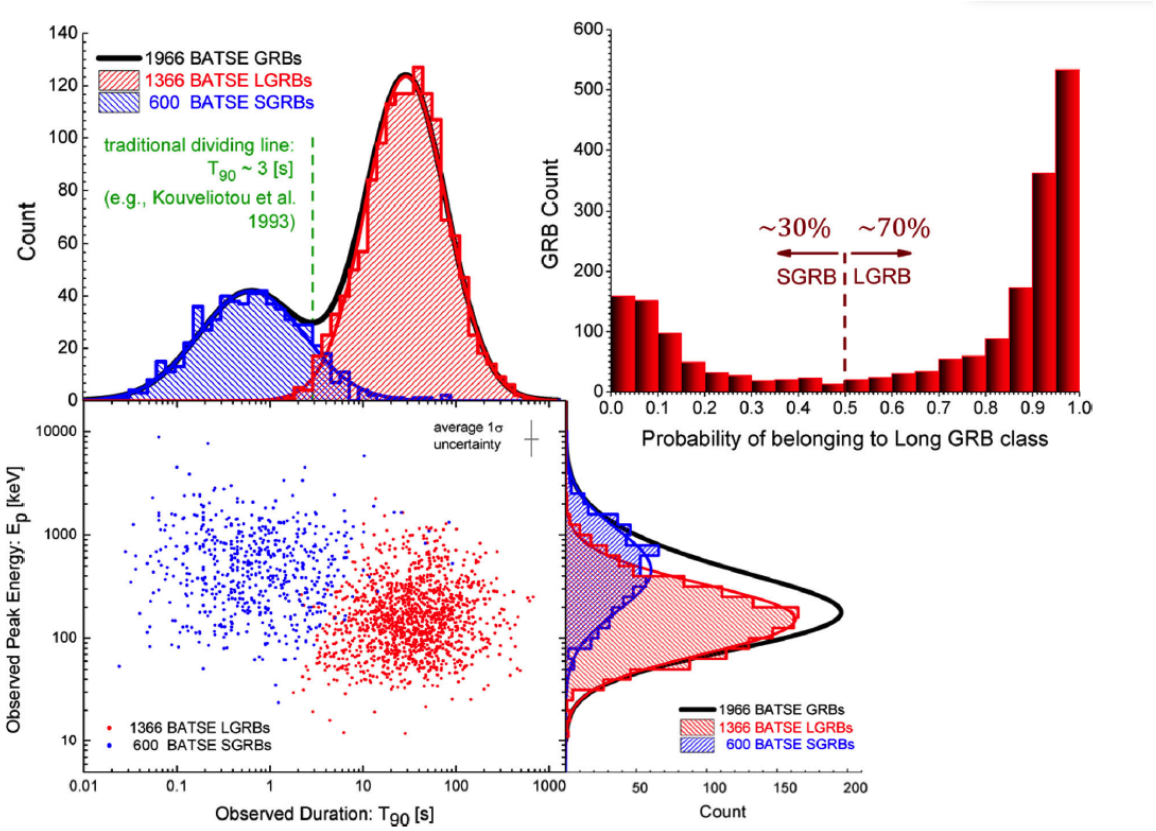

Figure 3.2: *Classification of BATSE GRB with measured peak flux, fluence, $T90$ (the duration over which 90 % of the total fluence is recorded), and measured spectral peak energies (E_p) exhibiting a bimodal distribution. The dashed vertical line shows the theoretical distinction between short and long GRB at two seconds. While there is a substantial overlap, this value is commonly used to distinguish between both distributions. This Figure was made by (Shahmoradi & Nemiroff, 2015).*

The merger of these compact objects occurs mainly by the loss of angular momentum and energy in the form of gravitational wave emission. In this scenario the expected remnant is a black hole surrounded by an accretion disk formed by the debris of the initial neutron stars that constitutes the main source of material for a kilonova ejected during the coalescence of these objects (Metzger et al., 2010). This kilonova, rich in neutrons, creates a significant amount of heavy elements through the rapid neutron capture process, or $r-$process (Tanvir et al., 2013; Lattimer & Schramm, 1974; Freiburghaus et al., 1999).

Only recently, with the detection of gravitational waves followed by the multi-frequency detection of the electromagnetic spectrum of the GW170817 event where two neutron stars merged, it was confirmed that, indeed, the progenitors of a sGRB are produced by this mechanism. (Sengupta, 2017).

During the coalescence of this binary system, the formation of a black hole initially preceded by a hyper$-$massive neutron star (HMNS) surrounded by a thick accretion disk is expected. This

HMNS can lose mass through various transport or dissipation mechanisms, such as dynamic ejection processes, expansion, cooling of the accretion disk, and neutrino-driven winds. Due to the density composition in the HMNS the mass loss is expected to be anisotropic (Rosswog & Ramirez-Ruiz, 2003). As a result, a neutrino-driven wind with MeV energies, similar to that ejected in other proto neutron stars, is expected. This wind has an angular dependence (see Figure 3.3) whose properties were previously studied in global simulations of the merger of two neutron stars (Perego et al., 2014).

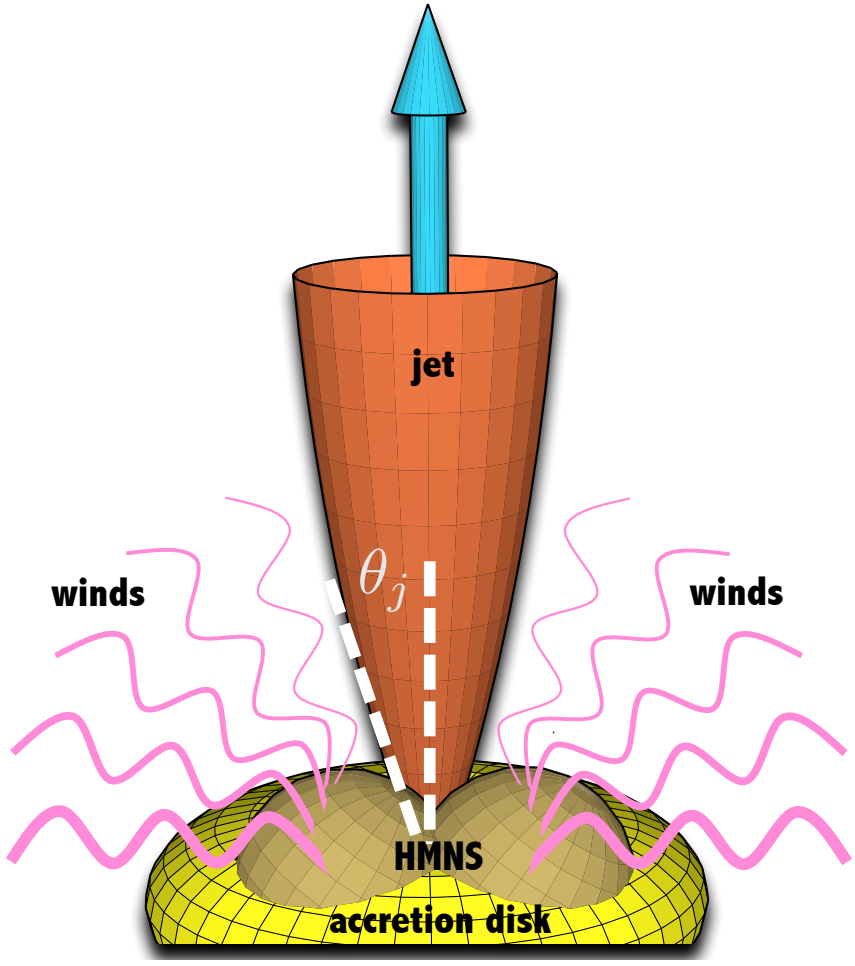

Figure 3.3: *Schematic view of the postmerger object (not to scale). In yellow, we display the accretion disk. The pink lines show the anisotropic distribution of winds that form around the central object with a markedly higher density at equatorial latitudes. For simplicity, the rotational axis is oriented on the jet propagation direction.*

3.3 Fireball model

In a GRB, the ejected material must be accelerated to relativistic velocities, which can only be accomplished by depositing a large amount of energy in a small region of space. This compact

source becomes so dense in energy that photons quickly form electron-positron pairs, which in turn annihilate to produce ultra-energetic gamma-rays. A "fireball" represents the initial mixing of particles and light caused by radiation so this model represents the link between a GRB's central engine and the progenitor envelope from which it emerges.

This fireball (initially opaque) contains a large concentration of radiation with an initial energy greater than its rest energy confined to a very small space where the baryonic mass is almost negligible. Initially, this model was proposed by Goodman and Paczinsky in 1986 (Goodman, 1986) and suggests that the observed radiation is produced by accelerating flow at relativistic velocities in the optically thin region. Although it may also be due to internal shocks or interaction with the interstellar medium (Rees & Meszaros, 1992), although the latter is unlikely because the process is very inefficient (Sari & Piran, 1997).

This fireball expands with a Lorentz factor of $\Gamma = (1 - (v/c)^2)^{-1} \sim 10^2 - 10^3$, reaching velocities v close to the speed of light (see Fig. 3.4). The majority of the radiation is released during this evolution by internal processes that occur when the outer layers, as they expand, begin to slow down and are reached by the inner layers colliding with each other. However, external processes can also release it when the outer layers interact with the interstellar medium.

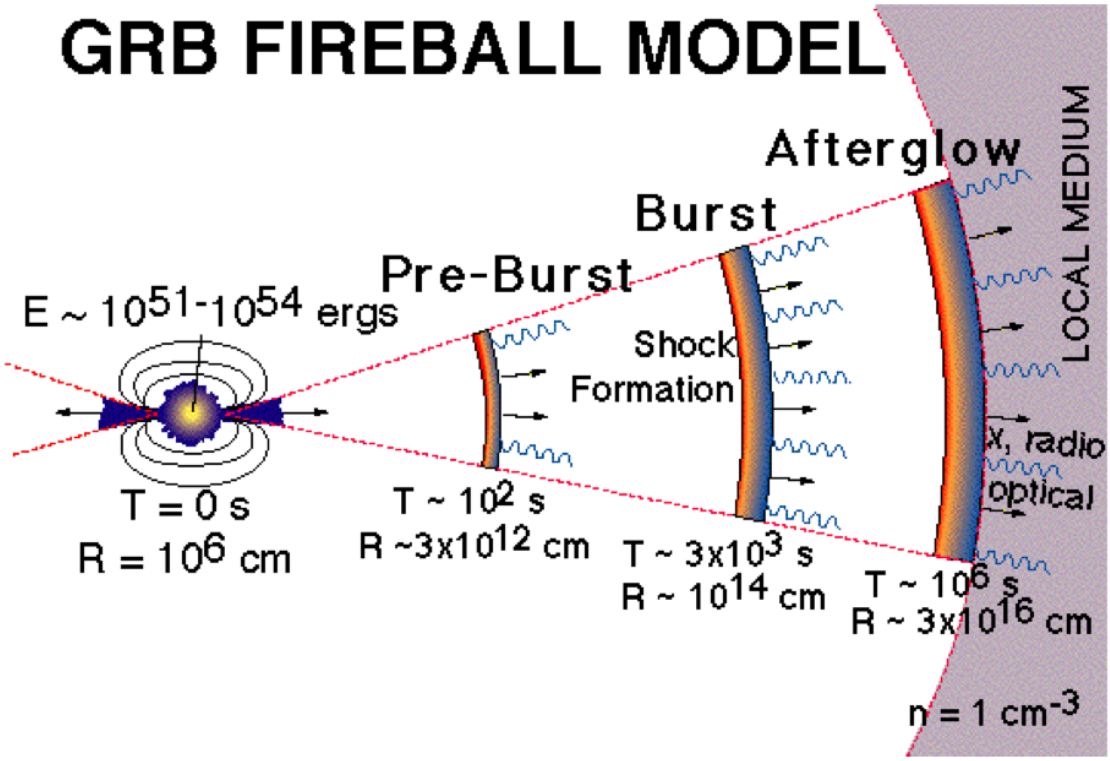

Figure 3.4: *Schematic representation for the GRB Fireball model. Credit: Gabriele Ghisellini.*

Although these neutrinos do not interact with matter directly, their properties can be modified indirectly when they propagate through a medium with a magnetic field, as each neutrino is

subjected to the action of an effective potential. Thus, understanding the magnetic field's effects on the expansion and cooling of a fireball is critical, as the magnetic field can be amplified by several orders of magnitude in some cases, reaching values of up to $B \sim 10^{17}$ G during the first millisecond (Price & Rosswog, 2006; Kyutoku & Kashiyama, 2018).

The fireball cools as it expands, reaching the temperature required for pair production, at which point it becomes optically thin. In the case of a "pure"[1] fireball, this occurs when the local temperature drops to $T \approx 20$ keV at $R_{\rm rad} \approx 10^{10}\ {\rm cm}\ {\rm E}_{52}^{1/4}{\rm R}_{\rm i,7}^{-3/4}$ or $t \approx (1/3)$ s (Piran, 1999), while the optical depth of a matter-dominated[2] fireball is usually determined by the surrounding electrons, and the fireball becomes optically thin at

$$R_e = \left(\frac{\sigma_T E}{4\pi m_p c^2 \eta}\right)^{1/2} \approx 6 \times 10^{13}\ {\rm cm}\sqrt{{\rm E}_{52}}\left(\frac{\eta}{100}\right)^{-1}\ , \tag{3.1}$$

where $\sigma_T = 6.6524 \times 10^{-25}\ {\rm cm}^2$ denotes the Thompson's cross-section, and $\eta \equiv E/Mc^2$. The expansion time which corresponds to this radius is $t \approx 2 \times 10^3$ s.

We rely on the most widely accepted fireball model to include GRB dynamics into our research. Because the temperature is higher than the rate of $e^{\pm}$ pair generation, nuclei are photodisintegrated, and the plasma is mostly made up of free $e^{\pm}$ pairs, γ-ray photons, and baryons. The base of the jet is generated by the so-called fireball plasma coupled to the progenitor. According to the fireball model, there will be two stages: the prompt emission: when jet inhomogeneities cause internal collisionless shocks (Rees & Meszaros, 1994; Fraija et al., 2017) and the afterglow: when the relativistic outflow sweeps up enough external material. In terms of progenitor models, later light curve measurements point to a "compact" inner engine, which can be described using this fireball model independently of the progenitor emission mechanism considered.

Initially, the fireball is opaque to neutrinos $\left(\tau_{\nu_e} = 54\ E_{52}^{5/4} r_{6.5}^{-11/4}\ {\rm and}\ \tau_{\nu_\mu} = 7.4\ {\rm E}_{52}^{5/4}{\rm r}_{6.5}^{-11/4}\right)$ (Koers & Wijers, 2005) but becomes transparent ($\tau_{\nu_e,\nu_\mu,\nu_\tau} < 1$) as it expands and then neutrinos can escape. Moreover, the fireball has strong magnetic fields and it is mainly composed of $e^{\pm}$ pairs and free nucleons that are basically at rest within the progenitor reference frame (Zhang & Meszaros, 2004). A quasi-thermal equilibrium is reached ($\sim 1 - 10$ MeV) within a typical size of $r = 10^{6.5} - 10^7$ cm, and densities of $10^9 \leq \rho \leq 10^{12}$ g cm^{-3}(Piran, 1999).

During this phase, a large number of thermal neutrinos are created inside the fireball plasma due to high temperatures and where the pair annihilation processes dominate $(e^+ + e^- \rightarrow \nu_x + \bar{\nu}_x)$.[3] However, other reactions, such as nucleon-nucleon bremsstrahlung $(NN \rightarrow NN + \nu_x + \bar{\nu}_x)$, plasma decay $(\gamma \rightarrow \nu_x + \bar{\nu}_x)$, positron capture on neutrons $(e^+ + n \rightarrow p + \bar{\nu}_e)$, and electron

[1] A fireball made exclusively of photons and leptons where the effect of baryons is insignificant in this scenario, and the fireball expands dominated by radiation ($E > mc^2$), with most of the energy escaping as radiation.

[2] Unlike a pure fireball, this one becomes matter-dominated before becoming optically thin. With Lorentz factor $\Gamma \approx (E/mc^2)$, most of the initial energy becomes the bulk kinetic energy of the baryons.

[3] The subindex x denotes that neutrinos of any flavor can be produced during these reactions $x = e, \mu, \tau$

capture on protons ($e^- + p \rightarrow n + \nu_e$), are also crucial for effective cooling of the system (Dicus, 1972). Since the latter reactions only produce neutrinos with a definite electron flavor, it is estimated that initially there is an over-proportion of this neutrino flavor. This effect will be considered later when we takes into account the initial flavor rates.

3.4 Afterglow

GRB remain visible at less intense wavelengths long after the original burst of gamma-rays has dissipated. This gradually fluctuating, low-energy radiation that can be observed days or months after a GRB is commonly known as the afterglow.

It is hypothesized that the afterglow derives from the external shock created when the explosion's blast wave collides and sweeps up material from the surrounding interstellar medium. This emission is synchrotron radiation, which occurs when electrons are accelerated in a magnetic field. The consecutive afterglows at gradually shorter wavelengths (X-ray, optical, radio) occur naturally when the expanding shock wave sweeps up more and more material, causing it to lose speed and energy and therefore slow down, resulting in even shorter afterglows (Levan, 2018).

From all GRB that have been detected to emit X-ray afterglows, roughly half also emit afterglows at optical and radio wavelengths. If no afterglow is seen at optical wavelengths, the GRB is referred to as a dark burst. However, recent research indicates that even dark bursts emit quickly fading afterglow radiation but it require very quick telescopes to spot it (Greiner et al., 2011).

Typical GRB afterglows are often described by four power-law segments separated by three break frequencies (Fig. 3.5)

The break frequencies are time-dependent. They are governed by the circumburst medium through which the fireball is traversing. The frequency at which synchrotron self-absorption becomes significant is denoted by the self-absorption break $\nu_a(t)$. The injection break frequency, $\nu_m(t)$, is the emission peak frequency of the electrons injected into the fireball. The cooling break, denoted as $\nu_c(t)$, is the peak emission frequency of an electron in a fireball within a cooling time scale.

3.5 Jets

Scientists initially assumed that GRB originated inside the galaxy since an extragalactic origin would need massive energy. When redshifts were ultimately calculated by monitoring optical afterglows in the 1990s, it became evident that GRB originated from outside our galaxy.

The subsequent challenge was to find a source capable of producing the $E = 10^{51} - 10^{54}$

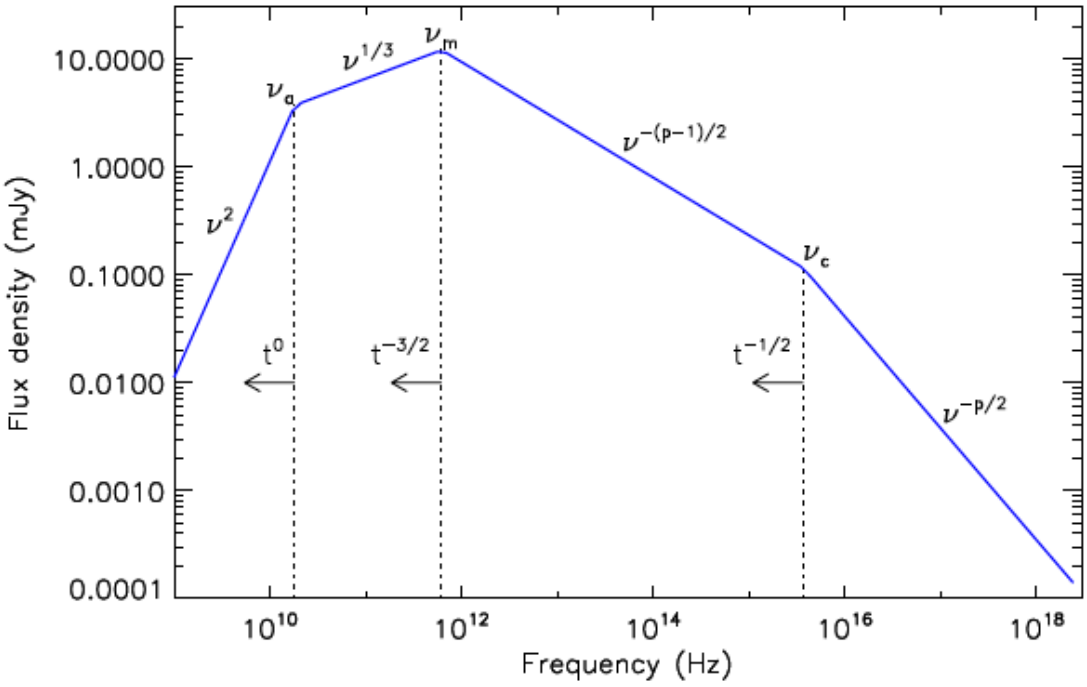

Figure 3.5: *Afterglow spectrum predicted from the fireball model in the slow-cooling regime. The diagram depicts the three break frequencies, evolution, and the spectral slopes. This figure was taken from (de Ugarte Postigo et al., 2012).*

erg of photon energy required to explain reported GRB luminosities. Popular explanations for the high luminosities of GRB presume that the emission is not isotropic but rather the outflow of a GRB is constrained to a collimated, double-sided jet with a half-opening angle of θ_j (Vedrenne G., 2010; Levan, 2018).

If GRB form jets, the actual energy of the burst should be significantly smaller than what would be predicted from an isotropic outflow because the emission is restricted to a slight solid angle.

$$E_K \approx (1 - \cos\theta_j)\ E_{\rm iso}\ , \tag{3.2}$$

where $E_{\rm iso}$ is the isotropic equivalent energy, and corresponds to the total kinetic energy of the burst under the assumption that it is isotropic. A jet's presence can generate a distinct signature in an afterglow light curve. When a jet is pointed directly at the observer, the viewer can only see the point center of the jet, but as the jet slows down, the beaming effect diminishes. The observer sees more and more of the jet's counterpart until the jet-break time $t_{\rm jet}$ is reached, at which point the observer can see the jet's edge. It is worth mentioning that jet breaks have been observed in several GRB afterglows.

According to the angle of view at which a GRB is observed, they are classified into *on-axis GRB* and *off-axis GRB*. On-axis GRB are gamma-ray bursts whose jet points directly toward the detector, i.e., for a viewing angle ($\theta_{\rm obs} < \theta_j$), where $\theta_{\rm obs}$ corresponds to the angle between

the observer and the jet emission line. A high luminosity characterizes this type of GRB due to the collimation of the electromagnetic radiation in the observer's direction. On the other hand, off-axis GRB are those gamma-ray bursts in which the prompt emission cannot be observed because the jet is not pointing directly at the detector. This occurs when the angle of observation is outside the range of view of the jet itself, such that ($\theta_{\rm obs} > \theta_j$).

3.6 Short Gamma-Ray Bursts

The stars participating in sGRB production are the remaining compact objects from massive stars' death in a binary configuration, black hole-neutron star or neutron-neutron star (hereafter, BH-NS and NS-NS, respectively). Because of angular momentum and radiation losses in gravitational waves, these star-type objects collide with each other on a temporal scale of milliseconds (Rosswog & Liebendörfer, 2003), generating a coalescence with exotic physical properties. When the compact objects are two NS, Kelvin-Helmholtz instabilities arise at the precise moment when both stars are close enough, promoting the amplification of the magnetic field by up to five orders of magnitude on the contact surface (Duncan & Thompson, 1992; Price & Rosswog, 2006; Zrake & MacFadyen, 2013; Kiuchi et al., 2014; Kiuchi et al., 2015). The result is a hyper massive neutron star (HMNS) surrounded by an accretion disk composed from the debris of both stars that can stand stable during a relatively long time or collapse into a black hole (Shibata & Taniguchi, 2006; Baiotti et al., 2008). According to Murguia-Berthier et al. (2014), the configuration of this hot and differentially-rotating structure requires that the mass of the HMNS lies in a range between the value of a cold and non-rotating structure and the maximum threshold for collapse toward a black hole, which is predicted to be $M_{\rm cold} \approx 2\ M_\odot < M_{\rm HMNS} < M_{\rm threshold} \approx 2.7\ M_\odot$ (Shibata & Taniguchi, 2006; Demorest et al., 2010). When the above inequality is fulfilled, many mechanisms may occur to dissipate and transmit energy and angular momentum, perhaps producing collapse after a delay of tens of milliseconds to a few seconds (Faber & Rasio, 2012).

During this process, baryonic winds are expelled outwards in a preferential direction towards the equatorial plane, forming a cloud density that initially can be opaque (see Figure 3.3). Moreover, for BH-NS mergers, the BH destroys the neutron star by tidal forces generating a tail from the stellar debris. Although the result will regularly be a black hole, several simulations have proved the existence of a hot, temporary, and deferentially rotating disk preceding the black hole formation, where these winds are also produced (Lee & Ramirez-Ruiz, 2007). In both cases, an accretion disk is formed around the progenitor with a vertical scale proportional to its radial size, temperatures of $T = 4$ MeV, and a period of rotation of ~ 1 ms.

3.6.1 Energy extraction mechanisms

Several extraction mechanisms have been developed in recent years to explain the more feasible cooling mechanisms for the post-burst debris. In that context, some authors have considered neutrino dominated accretion flows (NDAF) as responsible for releasing a large amount of energy through neutrino emission via $\nu\bar{\nu} \rightarrow e^+e^-$ processes in low-density regions (Popham

et al., 1999; Narayan et al., 2001; Di Matteo et al., 2002). In contrast, many others rely on MHD processes regarding the short timescales (Cheng & Lu, 2001; Koide & Arai, 2008). These mechanisms can be summarised into these two main groups, and we present them below.

$\nu\bar{\nu}-$ annihilation

In this scenario, neutrinos with energies $\sim$ 50 MeV are produced by pairs annihilation within the accretion disk (or around it). Initially, the disk is optically thick (reaching $\tau \sim 10^4$), and neutrinos look for a low-density region usually located in the funnel formed along the rotation axis; once there, the neutrino density gradient increases. Consequently, the annihilation rate grows to produce a fireball composed essentially of $(\gamma, e^{\pm})$. The fireball expands relativistically due to the low amount of baryonic material it has. In turn, the outflow of these neutrinos constitutes an effective mechanism for cooling the system, which drags and heats the surrounding baryonic medium into the so-called neutrino-driven winds (hereafter, NDW), which in principle is responsible for collimating the jet (Rosswog & Ramirez-Ruiz, 2002b). It is worth mentioning that part of the created energy by neutrinos is re-deposited into the disk in a colder flow ($T = 1$ MeV), continuing to feed the winds around the progenitor. Again, from the interactions with the baryonic material and the fireball's electrons, lower energy neutrinos are created. In fact, Rosswog & Liebendörfer (2003) found that neutrinos have an average energies of the order of ($E_\nu \simeq 8, 15, 20$-25) MeV for electronic, muonic and tauonic neutrinos, respectively. Unfortunately, the exact calculations of the wind density profiles are difficult to calculate and only recently were performed (e.g., see Dessart et al., 2008; Siegel et al., 2014; Perego et al., 2014).

MHD processes

The disadvantage of the previous mechanism is that it results in an extremely inefficient process because it requires a large neutrino luminosity or very short timescales (Ruffert et al., 1997); thus, other energy extraction mechanisms through MHD processes have also been proposed. That can be done either from the accretion disk during the HMNS stable phase or by rotational energy during the postmerger object collapse to a BH using the so-called Blandford-Znajek mechanism (Blandford & Znajek, 1977b; Daigne & Mochkovitch, 2002). In the first case, a toroidal magnetic field in the disk plane is formed, whose field lines are forced to reconnect quickly and then twisted due to the differential rotation of the disk and the magnetic field amplification. This process heats the surrounding medium, ejecting a wind outflow (Rosswog et al., 2003). In the second case, the energy extracted by the Blandford-Znajek mechanism is injected into the newly created winds from the disk debris through the Poynting flux before being converted into gamma rays. These winds tend to follow the magnetic field lines (Blandford & Payne, 1982). In all the conditions mentioned above, a very intense magnetic field ($B > 10^{15}$ G) is needed. Therefore, we will refer to magnetically-driven winds (hereafter, MDW) as those produced during a binary NS merger because this is the only known configuration where the magnetic field increases up to this intensity (Price & Rosswog, 2006; Giacomazzo et al., 2009; Kiuchi et al., 2014; Kiuchi et al., 2015).

3.7 LGRB and central engine models

It is believed that LGRB are formed as a result of massive star collapses and even though they have been studied for more than a half-century, much remains unknown about the dynamics of their progenitors. Several theories have been proposed to describe the possible central engines during this time period. So far, the most successful models are those that can describe the following characteristics observed during the prompt-emission and afterglow phases: i) the progenitors, in particular, must have a large energy reservoir capable of launching an ultra-relativistic outflow suitable for a GRB ($\sim 10^{49} - 10^{55}$ erg), ii) the source must last long enough with remarkable intermittency to match the variability of the observed X-ray light curves (Zhang et al., 2006; Troja et al., 2017), and iii) a large toroidal magnetic field is also expected in some cases, resulting in the formation of a magnetically-dominated outflow (Zhang & Pe'er, 2009). Within this framework, there are two promising progenitor models that meet these criteria. On the one hand, there is a black hole-disk system, and on the other, a millisecond magnetar, whose fast rotation required by the GRB central engine prevents its total collapse to a BH (Uso, 1992). A typical light curve explaining both events are shown in Figure (3.6) and a summary of these candidates' characteristics is provided below.
(Perego et al., 2014).

3.7.1 Black hole–accretion disk within the collapsar model

The collapsar model describes how a very massive star (typically larger than 30 $M_\odot$) (Podsiadlowski et al., 2004) loses hydrostatic equilibrium and succumbs to gravitational collapse in the core during its main-sequence evolution (Woosley, 1993b). During this phase, the star loses its external envelopes, which had a lot of angular momentum at the beginning. As a result, all the material in the star does not collapse directly into a black hole but rather forms a system consisting of a rotating black hole and an accretion disk. The gravitational potential energy contained is subsequently transformed into kinetic energy in the form of an ultra-relativistic jet along the rotating axis, while the accretion of surrounding material fuels the jet by either electrodynamic (Blandford & Znajek, 1977b) or neutrino-antineutrino annihilation processes (Ruffert et al., 1997; Popham et al., 1999; Chen & Beloborodov, 2007). Finally, the newly formed winds are injected from the torus debris via the Poynting flux before being converted into gamma rays.

The advantages of this model include that it can produce the high energy that has been recorded for some GRB. Still, it is difficult to explain the prolonged activity of the central engine that is sometimes found in certain X-ray light curves. Similarly, It is estimated that the inhomogeneous accretion of the BH-disk system tends to generate a steep decay rather than a smooth plateau (Du, 2020). The late accretion rate in this scenario follows a fall-back rate of $t^{-5/3}$, and the total energy is then determined either by the total accreted mass $E_{\rm tot} = \eta\ m_{\rm acc}c^2$ (Levan et al., 2016) or by the spin energy of the BH. In the first case, assuming an energy conversion efficiency factor $\eta = 0.1$ and an accretion mass of $\sim 10\ M_\odot$, the total energy is about $E_{\rm tot} \sim 2 \times 10^{54}$ erg. In the later case, the associated rotational energy of the black hole is also close to this value $E_{\rm rot} \sim 2 \times 10^{54}$ erg $f_{\rm rot}(a_\bullet)(M/M_\bullet)$, where $f_{\rm rot}(a_\bullet)$ represents a function in terms of the BH spin parameter $a_\bullet$ (Li et al., 2018). These

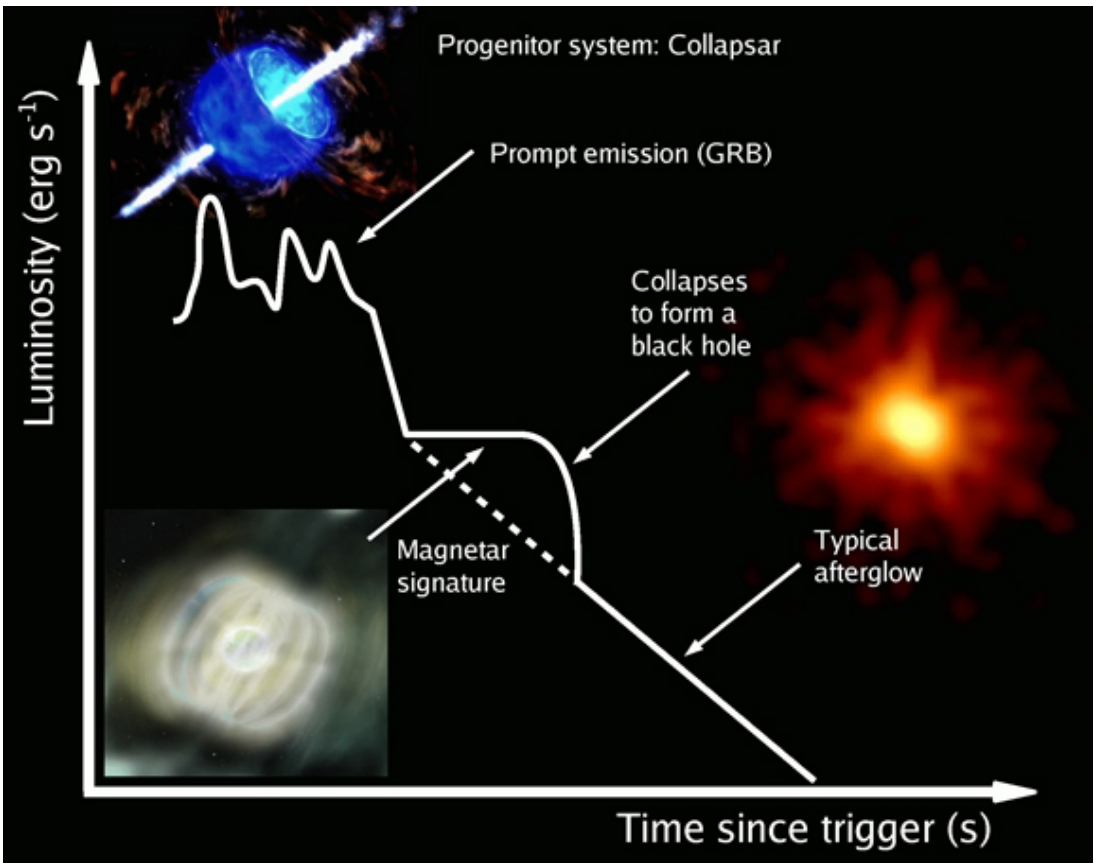

Figure 3.6: *Light curve of a LGRB, where the presence of a plateau-shaped magnetar signature is evident (solid line), compared to the expected observation of a core-collapse (dotted line). This Figure was made by (Rowlinson et al., 2011).*

values match the order of the most energetic GRB detected. Lastly, the associated magnetic field of the BH is estimated to be $\sim 10^{10} - 10^{12}$ G (Tsuruta et al., 2018; Moradi et al., 2021), depending on the energy extraction mechanism considered. In any case, these typical values are less than the critical magnetic field ($\Omega_B < 1$):

3.7.2 The millisecond magnetar model

In this scenario, a massive star first collapses to form a highly magnetized neutron star, converting all of the star's gravitational potential energy into rotational energy with a rotational period on the millisecond scale. When the magnetar is born, a plethora of neutrinos is produced via pair-annihilation eventually resulting in a fireball made primarily of leptons and photons. Because of the little amount of baryonic compound, the fireball expands relativistically. The neutrino outflow acts as an effective cooling mechanism for the system, dragging and heating the surrounding material in the so-called neutrino-driven winds. As a result, more neutrinos are created through the thermal interactions between baryons present in the winds and fireball electrons (cf. Section 3.3) with an average energy ranging about 8 and 25 MeV (Rosswog & Liebendörfer, 2003). For a magnetar-like magnetic field, this wind is accelerated by the dynamo mechanism and is more energetic than the first one, so the neutrino outflow is mag-

netically dominated throughout the cooling process (Thompson et al., 2004).

The primary benefit of this model is that it can account for a late energy injection into the burst. This model predicts a plateau phase in its X-ray light curves, which is attributed to the spin-down of a newly formed magnetar (Zhang et al., 2006; Troja et al., 2017). However, it poses a problem because the maximum amount of energy that can be extracted corresponds to the magnetar's rotational energy in this scenario. This can be calculated as (Lü & Zhang, 2014)

$$E_{rot} = \frac{1}{2} I \Omega_0^2 = \frac{2\pi^2 I}{P} \simeq 2.2 \times 10^{52} \text{ erg } M_{1.4} \, R_6^2 \, P_{0,-3}^2 \, , \tag{3.3}$$

assuming a canonical spherical NS with moment of inertia $I = \frac{2}{5} M R^2 \simeq 10^{45}$ g cm^{-2} $M_{1.4} \, R_6^2$ with initial angular frequency $\Omega_0 = \frac{2\pi}{P_0}$ and a period on a millisecond scale.

Even if some extreme massive values were taken into account, such as the hyper massive neutron stars near the *Tolman-Oppenheimer-Volkoff* (TOV) limit, the maximum energy budget could not exceed 8.5×10^{52} erg. This represents a problem because many GRB have been observed with energy reservoirs greater than this value. Typically, these GRB have been linked to a BH central engine capable of delivering such a large amount of energy.

3.8 Central Compact Objects (CCO)

Central compact objects (CCO) are a subgroup of neutron stars with thermal spectra that have been observed at galactic distances. The dipolar component of the external magnetic field at the pole is estimated to be $B_p \equiv 3.2 \times 10^{19} \, (P\dot{P})^{1/2} \sim 10^{10}$ G. This magnetic field strength is atypically low compared to other pulsars (Viganò & Pons, 2012; Luo et al., 2015) as had originally been predicted by (Muslimov & Page, 1995; Geppert et al., 1999).

These sources must meet the following classification criteria to be considered CCO: i) they are in a region near the center of young supernova remnants (0.3-7 kyr); ii) they have no radio or optical counterparts; iii) they do not have detectable pulsar wind nebulae; iv) they have a thermal spectrum in the soft X-ray band with a typical luminosity between $L_X = 10^{32} - 10^{33}$ erg s^{-1}; and v) Blackbody functions with temperatures ranging from 0.2 to 0.6 keV can describe the spectral distribution of these sources.

At the moment, nine CCO have been confirmed, of which only the following are studied in this work: i) RXJ0822-4300; ii) XMMU J173203.3-344518; iii) 1E 1207.4-5209; iv) CXOU J160103-513353; v) 1WGA J1713.4-3949; vi) XMMU J172054.5-372652; and vii) CXOU J085201.4-461753.

3.9 Strange Stars (SS)

Strange stars are a subgroup of quark stars formed by strange quarks, the so-called strange quark matter (SQM). It is believed that such sources could originate during the first seconds

after the core collapse or during the binary merger of a compact object by interaction with a strange star (SS-BH, SS-NS, SS-SS) (Alcock et al., 1986; Olinto, 1987).

According to the MIT-Bag model[4], it is known that the negatively charged SQM (SQM^-) is not stable in a pressureless environment. During the merger of two compact objects in which at least one of them corresponds to a strange star, some strangelets could escape and interact with ordinary matter. Then there would be no Coulomb barrier to prevent the normal matter from being converted into SQM. Furthermore, these strangelets have the potential to convert entire planets or stars into strange matter on a larger scale that has not been observed. As a result, if SQM^- exists, we assume it can only exist at high pressures and be surrounded by SQM^+ (positively charged SQM), as shown in Fig. (3.7).

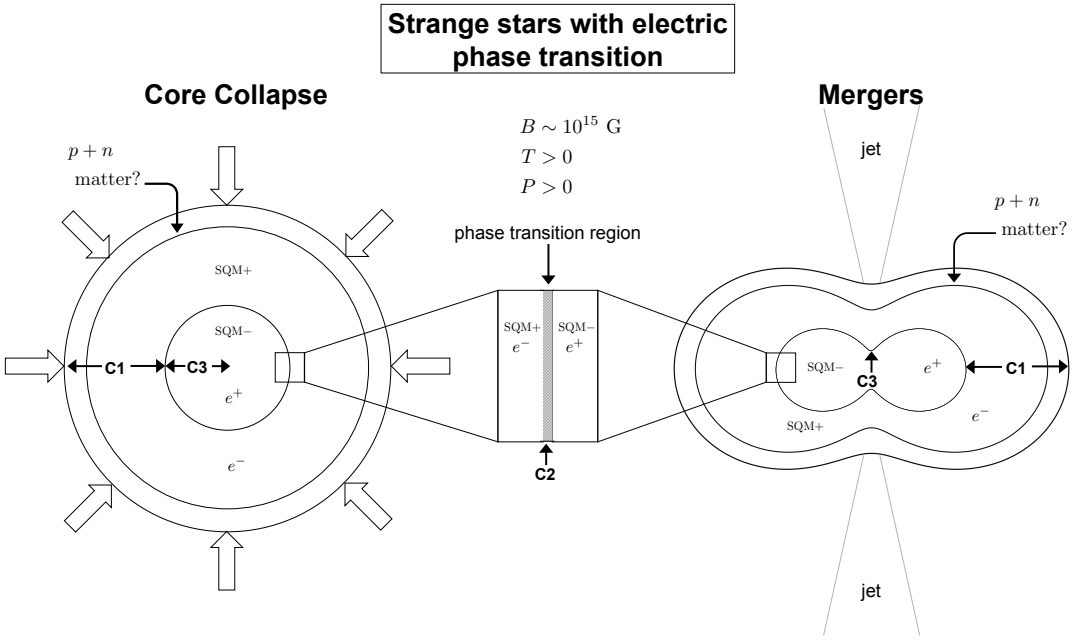

Figure 3.7: *We provide a schematic view of a SS with the electric phase transition between SQM^+ and SQM^- during the core-collapse on the left-hand side of the diagram. The region surrounding the phase transition (C2) is zoomed in near the diagram's center. The identical C2 region is depicted on the right-hand side of the diagram during a binary SS merger. SQM^- area C1 may exist at zero pressure, whereas SQM^- region C3 may only exist at finite pressure within a SS. C1 would occupy the entire compact object if no electric phase transition exists.*

After the baryon density exceeds ($n_{\rm bar} = 0.6$), electrons are replaced by positrons, as Fraija & Méndez (2014) demonstrated. In this scenario, a zone where pairs annihilate into neutrinos may form. Neutrinos can be created in this area even when the strange matter has cooled below 1 MeV and the charge neutrality must be established locally. Thus, beta equilibrium must provide electrons (positrons) to replace those destroyed at the ($SQM^+ - SQM^-$) interface

[4]In this model, quarks are forced to be confined in a limited region of space by an external force (in this case, gravitational), occupying single-particle orbitals (Glendenning, 2012).

where SQM$^+$ (SQM$^-$) exists. As a result of these beta-equilibrium processes, a large amount of thermal neutrinos (antineutrinos) will be produced.

Limiting the total mass lost to neutrino cooling of a compact star (NS or SS) to half a solar mass (an overestimate even for the most massive ones) provides us with $E_\nu \sim (10^{33}\,\mathrm{g}) \sim 10^{54}\,\mathrm{erg}$. According to Page et al. (2004, 2011) the $\nu-$cooling timescale may be as long as a few

$$\tau_\nu \sim 10^6 \mathrm{yr} \sim \pi \times 10^{13} \mathrm{s}, \tag{3.4}$$

thus allowing for a neutrino luminosity of up to

$$L_\nu = E_\nu/\tau_\nu \sim 10^{40} \mathrm{erg\ s^{-1}}. \tag{3.5}$$

This energy and luminosity budgets must be shared between the beta equilibrium reactions between the quarks up (u), down (d) and strange (s) occurring throughout the star:

- SQM$^+$:

$$u + e^- \rightarrow d + \nu_e \qquad d \rightarrow u + e^- + \bar{\nu}_e u + e^- \rightarrow s + \nu_e \qquad s \rightarrow u + e^- + \bar{\nu}_e$$

- SQM$^-$:

$$d + e^+ \rightarrow u + \bar{\nu}_e \qquad u \rightarrow d + e^+ + \nu_e s + e^+ \rightarrow u + \bar{\nu}_e \qquad u \rightarrow s + e^+ + \nu_e$$

and $e^\pm$ pair annihilation at the SQM$^+$–SQM$^-$ interface region:

- $e^\pm$ pair annihilation:

$$e^+ + e^- \rightarrow \nu_x + \bar{\nu}_x. \tag{3.6}$$

4 Scientific articles

4.1 Preface

This chapter is a collection of articles that I have developed during my Ph.D. research. The theories and unknowns addressed in these publications are diverse, but they were all conceived with the aim of obtaining as much information as possible from neutrino emitting sources by examining the particle characteristics and their evolution when they propagate towards Earth.

The first three articles are based on papers in which I am a corresponding author and have already been published.

I include the latter three since they pertain to the topic but are applicable to different types of astrophysical sources. I only have a minority participation in the scientific development of these articles. In essence, I contributed to these papers by performing certain numerical calculations, creating Figures, and partially authoring certain sections.

1. **Morales, G.**, & Fraija, N. (2021). *Neutrino propagation in winds around the central engine of sGRB.* Monthly Notices of the Royal Astronomical Society, 505(4), 4968-4980. DOI: https://doi.org/10.1093/mnras/stab1577.

2. **Morales, G.**, & Fraija, N. (2021). *Differentiating short gamma-ray bursts progenitors through multi-MeV neutrinos.* Journal of High Energy Astrophysics, 32, 87-101. DOI: https://doi.org/10.1016/j.jheap.2021.09.001.

3. **Morales, G.** & Fraija, N. (2022). *On LGRB progenitors: an approach from thermally-produced neutrinos*. Journal of High Energy Astrophysics, 34, 217-228. DOI: https://doi.org/10.1016/j.jheap.2022.05.004.

4. Fraija, N., Bernal, C. G., **Morales, G.**, & Negreiros, R. (2018). *Could a Hypercritical Accretion be Associated with the Atypical Magnetic-field Behavior in RX J0822-4300?*. Publications of the Astronomical Society of the Pacific, 130(994), 124201. DOI: https://doi.org/10.1088/1538-3873/aae1d3.

5. Fraija, N., Bernal, C. G., **Morales, G.**, & Negreiros, R. (2018). *Hypercritical accretion scenario in central compact objects accompanied with an expected neutrino burst.* Physical Review D, 98(8), 083012.
DOI: https://doi.org/10.1103/PhysRevD.98.083012.

6. Fraija, N., Méndez, E. M., **Morales, G.**, & Saracho, A. (2022). *Neutrino Signal from Compact Objects during their Formation, their Mergers, or as a Signature of Electric-Charge Phase Transition*, Submitted to New Astronomy.
arXiv: https://arxiv.org/abs/1905.00575.

It is worth noting that the full versions of the aforementioned articles are supplied towards the end of this thesis to improve readability.

4.2 First article

Motivation

In the first manuscript, we studied the propagation of neutrinos through the winds produced during the formation of a short GRB. We wanted to address this problem because, in the past, several authors had often considered this wind to be isotropic or not even considered it at all. This is because obtaining density profiles describing the ejection of this material had been a problem for many years since a reliable description implied the use of relativistic hydrodynamic (or even MHD) simulations that required much computational power. A complete analysis of these scenarios was only recently taken into account in the work of (Perego et al., 2014) (neutrino-driven winds) and (Siegel et al., 2014) (magnetically-produced winds), where these effects were incorporated considering various mechanisms of energy extraction and wind production.

The most outstanding result of these works is that the density profile of these winds was not isotropic but had an angular variation of more than three orders of magnitude between both cases (as can be seen in Figure 2 of this article). As expected, this contribution is smaller for polar latitudes and larger at latitudes close to the plane of the equator due to the contribution provided by the accretion disk. With these results, we came up with the idea of analyzing the evolution of the properties of neutrinos propagating within these media, and so we proceeded as follows.

The neutrino oscillations must incorporate the effects of the medium through the effective potential, which could be calculated through the density profiles of both magnetically and neutrino-driven winds. First, we had to demonstrate that the propagation of neutrinos within these winds is adiabatic. We then proceeded to obtain the neutrino oscillation probabilities within both media. Further analysis of the variability of the probabilities concerning propagation latitude for a range of energies between 1 and 30 MeV was presented in oscillograms for both cases. This also allowed us to calculate the expected neutrino rates as a function of E_ν and θ_j, which we compared with the theoretical probabilities we would expect to obtain in the vacuum. The joint analysis of these results, but mainly the particular behavior deduced from

the expected rates (Figure 12), would allow us to determine the energy extraction mechanism through which the baryonic winds surrounding the central engine were created.

Contribution

The idea for this paper was developed jointly with N. Fraija as a natural consequence of using neutrino evolution to describe these media with physically quantifiable attributes. My goal was to show that the adiabaticity condition is satisfied for density profiles with these characteristics and that the neutrino energies considered are within the energy range where matter effects are dominant. In addition to the traditional calculations of the oscillation probabilities, I proposed the idea of representing the oscillation probabilities in a contour plot ($E_\nu - \theta_j$) to exhibit the dependence with respect to these variables within both scenarios. I also employed a new way to parameterize the neutrino rates and to present the ternary plots as a tool for determining the allowed range of oscillation. I was primarily responsible for the writing procedure (in LaTeX), numerical calculations, and Figures.

4.3 Second article

Motivation

In the second manuscript, we wanted to use neutrinos once more as a tool to characterize the previously identified sGRB progenitors (the merger of two compact objects in a black hole-neutron star or binary NS configuration). In this sense, the emphasis was on studying the evolution of these particles from their creation in a magnetized fireball to their possible detection on Earth with future neutrino telescopes. The main difference between this paper and the previous one is that the effective neutrino potential was calculated using Feynman diagrams of neutrino self–energy, which take into account the effects of the medium such as magnetic field, chemical potential, neutrino energy, neutrino propagation angle, and temperature. We also obtained neutrino resonance lengths and energies for a fireball with these properties, demonstrating that the medium has a strong influence on neutrino properties.

We calculated the expected neutrino rates after calculating the oscillation probabilities for both media. As an additional contribution, we expressed neutrino opacity as a function of propagation angle, discovering that only in the case of magnetic field amplification (binary NS mergers) does the surrounding medium become opaque to neutrinos when they propagate at latitudes greater than 62° with respect to the jet propagation axis (half-opening angle).

With this result, we could, in principle, differentiate between both progenitors because if we can detect a sGRB while also determining that it was emitted off–axis (with a line of sight greater than the critical angle of 62 degrees), we can conclude that this sGRB was produced during a BH–NS merger transparent to neutrinos because otherwise, the opacity of a medium with magnetic field amplification (NS–NS) would have prevented us from observing it. Finally, we estimate the detectability of these MeV neutrinos in future detectors, discovering that Hyper–Kamiokande is the most promising experiment among all.

Contribution

My advisor helped lay the foundation for this article. The two authors equally shared the responsibility for scientific development and writing (in LaTeX). N. Fraija derived the formula for the neutrino potential in this medium while I made the figures and numerical calculations.

4.4 Third article

Motivation

The idea of developing this article was developed jointly with N. Fraija, grouping the ideas that we developed in the first two articles but towards the two central engine models for LGRB that currently exist; accretion disk black hole and millisecond magnetar. In this work, we considered the distinctive characteristics of the medium developed under each LGRB central engine model that would undoubtedly influence the dynamics of the neutrinos produced and propagated in each type of source. We intended to find these variations and quantify them in both scenarios to characterize both progenitors' properties. Contrary to what was proposed in Article 2, in the magnetar regime, observations show that the magnetic field strength is not as high as that reached during magnetic field amplification in a NS merger. However, it is strong enough to use the effective neutrino potential within a regime that exceeds the critical magnetic field ($\Omega_B > 1$). At the same time, we consider a potential with a magnetic field ($\Omega_B < 1$) for a system composed of an accretion disk-black hole. We reproduced the neutrino oscillations in a fireball within these two scenarios and derived flavor-dependent rates with these bases. We thought this study in this field was critical because it is currently thought that there are a large number of unknown or hidden sources that could contribute to the observed diffuse neutrino flux or that there are simply some sources where no electromagnetic counterpart is expected (as in failed GRB) and these analysis can help us distinguish between both models.

Finally, we estimate the number of neutrinos expected in the Hyper-Kamiokande detector for a collection of past events that have been associated with a magnetar-like progenitor based on their characteristics. In order to detect these neutrinos, we discovered that a combination of ideal conditions (sufficiently energetic and close emitting sources) is required, particularly for this detector.

Contribution

The scientific development was divided equally between the two authors. The numerical calculations, the Figures, and the writing procedure (in LaTeX) were mainly carried out by me.

4.5 Fourth article

Motivation

For this paper, we investigated, among other things, the thermal neutrino oscillations produced by the pulsar RX J0822.4300 during its hypercritical accretion phase inside the supernova

remnant Puppis A. To account for these effects, we had to build the effective potential for each of the four known regions within this model. Using a slab approximation, the dynamics of neutrino evolution through these regions toward the Earth were integrated by neutrino oscillations in each model region. Subsequently, a flavor ratio was obtained and the number of expected events in three detectors; Super-Kamiokande, DUNE, and Hyper-Kamiokande were calculated. We show that the detection of a high number of neutrinos is expected for this type of central compact object due to the large neutrino flux expected from this galactic source located only 2.2 kpc away.

Contribution

The idea and scientific development were primarily made by N. Fraija and C. G. Bernal. I contributed in writing some paragraphs of the manuscript in LaTeX. Additionally, I did some numerical calculations and Figures within the article.

4.6 Fifth article

Motivation

Similar to Article 4, the neutrino calculations were reproduced, but this time they were applied to all CCO sources with known redshift at the time. In other words, it could be seen as broadening the previous paper, which only looked at one known source. This enabled us to conduct a statistical analysis of the hyper accretion regime, concluding that a slight deviation from the expected neutrino rate (1:1:1) is expected in all sources and that the neutrino burst corresponds to the only evidence for the existence of the post-core-collapse hypercritical phase in the supernova, which is responsible for explaining the anomalous low magnetic field found in CCO.

Contribution

My contribution to this article was similar to the one mentioned in article 4.

4.7 Sixth article

Motivation

The goal of this paper was to look into the evolution of neutrinos in a magnetized plasma made up of nuclear matter with a high nucleon number in the form of strange quark matter SQM for a positively charged environment made up only of electrons (SQM+), a negatively charged environment made up only of positrons (SQM-), and the electric interphase transition between the two regions. Neutrinos generated within this medium were discovered to oscillate resonantly in all three regions studied. Thermal neutrinos detected from these sources are a signature of the pair annihilation cooling mechanism during an electric charge phase transition. Because charged particles ($e^{\pm}$) are confined to Landau levels, the neutrinos produced during pair annihilation in the electric phase transition will be aligned preferentially to the local

magnetic field lines. Thus, studying the angular variation during neutrino propagation could infer the geometry of the magnetic field within this scenario, which would be impossible to describe using other mechanisms.

Contribution

N. Fraija and E. Moreno were primarily responsible for the idea and scientific development. I made the Figures in this article and some of the numerical calculations.

5

Conclusions

Neutrinos by nature are quite remarkable particles that could explore the astrophysical sources mainly because these particles originate in a very hot medium. They travel towards the Earth through a dense column density. We showed that once neutrinos transit a non-vacuum medium, their oscillation probabilities are affected by the surrounding medium but mainly by the magnetic component. So we were able to characterize the central engine associated with these events by studying and recognizing these variations. The following is a compilation of the most significant conclusions. It should be mentioned that further information on these conclusions can be found at the end of each paper.

- Neutrinos are an additional mechanism for discriminating the GRB progenitors. They can also help determine whether a GRB is seen on-axis or off-axis. This becomes more relevant when, for example, the sources are initially opaque to photons but transparent to neutrinos, or there is no electromagnetic counterpart at all. Since currently, there are additional candidate sources that could contribute to the observed diffuse neutrino flux.

- During the coalescence of two neutron stars, neutrinos cannot escape for propagation at half-opening angles greater than ~ 62 degrees. For these latitudes, the density of the baryonic material surrounding the postmerger remnant is so high that the medium becomes opaque to neutrinos.

- With the quantifiable attributes that future detectors could collect from these particles, we could reconstruct the internal topology of the emitting sources and the production mechanism.

- In the beginning, the joint detection of neutrinos and the EM channel is expected to be dependent in order to correlate the source, determine position, distance, and estimated neutrino flux. In an ideal scenario, however, we would expect that after statistically analyzing a number of these detections, we could infer the type of progenitor associated with each event based on the proportion of neutrino flavors detected without the help of the EM counterpart.

- CCO are astrophysical sources that are less energetic and have less magnetic activity than GRB. Despite this, it is expected that Hyper-K can detect about $\sim 10^3$ neutrinos due to the closeness of these events within the galactic plane. With a higher incidence, it is possible to make a more reliable statistical analysis to prove the existence of the hypercritical phase and explain the anomalous magnetic field present in these sources ($B_p \sim 10^{10}$ G).

- GRB have several orders of magnitude more energy than CCO, but they are found at extragalactic distances. As a result, some requirements (nearby and powerful enough with a reasonable flux of neutrinos) must be fulfilled for future detectors to detect them.

- The number of neutrino events for the current Super-K and the future DUNE and Hyper-K detectors was computed. In addition, more giant mega detectors, such as Deep-TITAND (5 Mton) and MICA (10 Mton), are also planned for the further future, which would increase the detection capability of these particles and for which we have not performed estimations in this work.

- Despite having reproduced the calculations of neutrino oscillations considering the normal and inverted hierarchy parameters, the discrepancies between the two scenarios were negligible for our analysis.

- It is undeniable that theoretical models that are compatible with observational data are required. With the aid of improved mega detectors in the coming years and the ongoing development of neutrino physics, a significant breakthrough in this field is expected, guiding us to a better grasp of the fundamental physics that governs the most extreme events in the Universe.

Bibliography

Abbott B. P., et al., 2017, Physical Review Letters, 119, 161101

Abe K., et al., 2011, Letter of Intent: The Hyper-Kamiokande Experiment — Detector Design and Physics Potential — (arXiv:1109.3262)

Abe K., et al., 2018a, arXiv preprint arXiv:1805.04163

Abe K., et al., 2018b, Progress of Theoretical and Experimental Physics, 2018, 063C01

Abe K., et al., 2022, Nuclear Instruments and Methods in Physics Research Section A: Accelerators, Spectrometers, Detectors and Associated Equipment, 1027, 166248

Acciarri R., et al., 2016, arXiv preprint arXiv:1601.02984

Ackermann M., et al., 2013a, The Astrophysical Journal Supplement Series, 209, 11

Ackermann M., et al., 2013b, The Astrophysical Journal Supplement Series, 209, 34

Adams C., et al., 2013, arXiv preprint arXiv:1307.7335

Alcock C., Farhi E., Olinto A., 1986, The Astrophysical Journal, 310, 261

Bahcall J. N., 1989, Neutrino astrophysics. Cambridge University Press

Baiotti L., Giacomazzo B., Rezzolla L., 2008, Phys. Rev. D, 78, 084033

Barger V., Whisnant K., Phillips R. J. N., 1980, Phys. Rev. D, 22, 1636

Barthelmy S. D., et al., 2005, Space Science Reviews, 120, 143

Beacom J. F., Vagins M. R., 2004, Physical review letters, 93, 171101

Becker J. K., 2008, Physics Reports, 458, 173

Berger E., 2014, Annual Review of Astronomy and Astrophysics, 52, 43

Bilenky S., 2010, Introduction to the Physics of Massive and Mixed Neutrinos, 1 edn. Lecture Notes in Physics 817, Springer-Verlag Berlin Heidelberg

Blandford R. D., Payne D. G., 1982, MNRAS, 199, 883

Blandford R. D., Znajek R. L., 1977a, MNRAS, 179, 433

Blandford R. D., Znajek R. L., 1977b, MNRAS, 179, 433

Bloom J. S., 2011, What Are Gamma-Ray Bursts. PUP

Chen W.-X., Beloborodov A. M., 2007, The Astrophysical Journal, 657, 383

Cheng K., Lu Y., 2001, Monthly Notices of the Royal Astronomical Society, 320, 235

Chevalier R. A., Li Z.-Y., 1999, The Astrophysical Journal Letters, 520, L29

Costa E., et al., 1997, Nature, 387, 783

Daigne F., Mochkovitch R., 2002, A&A, 388, 189

Danby G., Gaillard J. M., Goulianos K., Lederman L. M., Mistry N., Schwartz M., Steinberger J., 1962, Physical Review Letters, 9, 36

De Gouvêa A., Martinez-Soler I., Perez-Gonzalez Y. F., Sen M., 2020, Physical Review D, 102, 123012

Demorest P. B., Pennucci T., Ransom S., Roberts M., Hessels J., 2010, nature, 467, 1081

Dessart L., Ott C., Burrows A., Rosswog S., Livne E., 2008, The Astrophysical Journal, 690, 1681

Di Matteo T., Perna R., Narayan R., 2002, The Astrophysical Journal, 579, 706

Dicus D. A., 1972, Phys. Rev. D, 6, 941

Dighe A. S., Smirnov A. Y., 2000, Phys. Rev. D, 62, 033007

Du S., 2020, The Astrophysical Journal, 901, 75

Duncan R. C., Thompson C., 1992, ApJL, 392, L9

Eichler D., Livio M., Piran T., Schramm D. N., 1989, Nature, 340, 126

Faber J. A., Rasio F. A., 2012, Living Reviews in Relativity, 15, 1

Fishman G. J., et al., 1993, A&AS, 97, 17

Fraija N., 2010, PhD thesis, Universidad Nacional Autónoma de México

Fraija N., 2014, The Astrophysical Journal, 787, 140

Fraija N., Méndez E. M., 2014, arXiv preprint arXiv:1401.3787

Fraija N., Bernal C. G., Hidalgo-Gaméz A. M., 2014, MNRAS, 442, 239

Fraija N., et al., 2017, ApJ, 848, 15

Freiburghaus C., Rosswog S., Thielemann F.-K., 1999, The Astrophysical Journal Letters, 525, L121

Fukuda S., et al., 2003, Nuclear Instruments and Methods in Physics Research Section A: Accelerators, Spectrometers, Detectors and Associated Equipment, 501, 418

Gell-Mann M., Pais A., 1955, Phys. Rev., 97, 1387

Geppert U., Page D., Zannias T., 1999, Astronomy and Astrophysics, 345, 847

Giacomazzo B., Rezzolla L., Baiotti L., 2009, MNRAS, 399, L164

Giunti C., Kim C. W., 2007, Fundamentals of Neutrino Physics and Astrophysics, illustrated edition edn. Oxford University Press, USA

Glendenning N. K., 2012, Compact stars: Nuclear physics, particle physics and general relativity. Springer Science & Business Media

Goldstein A., et al., 2012, The Astrophysical Journal Supplement Series, 199, 19

Goldstein A., et al., 2017, The Astrophysical Journal Letters, 848, L14

Gonzalez-Garcia M. C., Nir Y., 2003, Reviews of Modern Physics, 75, 345

Goodman J., 1986, ApJL, 308, L47

Goodman M., 2015, Advances in High Energy Physics, 2015

Greiner J., et al., 2011, Astronomy & Astrophysics, 526, A30

Grindlay J., Zwart S. P., McMillan S., 2006, Nature Physics, 2, 116

Gross D. J., Wilczek F., 1974, Physical Review D, 9, 980

Halzen F., 2007, Ap&SS, 309, 407

Hartmann D. H., 1999, Proceedings of the National Academy of Sciences, 96, 4752

Jarlskog C., 1985, Phys. Rev. Lett., 55, 1039

Kann D., et al., 2010, The Astrophysical Journal, 720, 1513

Kiuchi K., Kyutoku K., Sekiguchi Y., Shibata M., Wada T., 2014, Phys. Rev. D, 90, 041502

Kiuchi K., Cerdá-Durán P., Kyutoku K., Sekiguchi Y., Shibata M., 2015, Phys. Rev. D, 92, 124034

Klebesadel R. W., Laros J. G., Fenimore E. E., 1984, in Bulletin of the American Astronomical Society. p. 1016

Kochanek C. S., Piran T., 1993, arXiv preprint astro-ph/9305015

Kodama K., et al., 2001, Physics Letters B, 504, 218

Koers H. B. J., Wijers R. A. M. J., 2005, MNRAS, 364, 934

Koide S., Arai K., 2008, The Astrophysical Journal, 682, 1124

Krimm H. A., et al., 2013, The Astrophysical Journal Supplement Series, 209, 14

Kudenko Y., 2020, Journal of Instrumentation, 15, C07029

Kyutoku K., Kashiyama K., 2018, Phys. Rev. D, 97, 103001

Lattimer J. M., Schramm D. N., 1974, ApJL, 192, L145

Lattimer J. M., Schramm D. N., 1976, The Astrophysical Journal, 210, 549

Lee W. H., Ramirez-Ruiz E., 2007, New Journal of Physics, 9, 17

Levan A., 2018, Gamma-Ray Bursts. 2514-3433, IOP Publishing, doi:10.1088/2514-3433/aae164, https://dx.doi.org/10.1088/2514-3433/aae164

Levan A., Crowther P., de Grijs R., Langer N., Xu D., Yoon S.-C., 2016, Space Science Reviews, 202, 33

Li L., Wu X.-F., Lei W.-H., Dai Z.-G., Liang E.-W., Ryde F., 2018, The Astrophysical Journal Supplement Series, 236, 26

Lü H.-J., Zhang B., 2014, The Astrophysical Journal, 785, 74

Lunardini C., 2016, Astroparticle Physics, 79, 49

Luo J., Ng C.-Y., Ho W. C. G., Bogdanov S., Kaspi V. M., He C., 2015, The Astrophysical Journal, 808, 130

MacFadyen A., Woosley S., 1999, The Astrophysical Journal, 524, 262

Maki Z., Nakagawa M., Sakata S., 1962, Progress of Theoretical Physics, 28, 870

Meegan C., Fishman G., Wilson R., Paciesas W., Pendleton G., Horack J., Brock M., Kouveliotou C., 1992, Nature, 355, 143

Meier D. L., Koide S., Uchida Y., 2001, Science, 291, 84

Mészáros P., 2000, Nuclear Physics B-Proceedings Supplements, 80, 63

Meszaros P., Rees M., 1993, The Astrophysical Journal, 405, 278

Metzger B. D., et al., 2010, Monthly Notices of the Royal Astronomical Society, 406, 2650

Mohapatra R. N., Pal P. B., 2004, Massive neutrinos in physics and astrophysics

Moradi R., Rueda J. A., Ruffini R., Wang Y., 2021, A&A, 649, A75

Murguia-Berthier A., Montes G., Ramirez-Ruiz E., De Colle F., Lee W. H., 2014, The Astrophysical Journal Letters, 788, L8

Muslimov A., Page D., 1995, The Astrophysical Journal, 440, L77

Nakar E., Piran T., Granot J., 2002, The Astrophysical Journal, 579, 699

Narayan R., Piran T., Kumar P., 2001, ApJ, 557, 949

Olinto A. V., 1987, Physics Letters B, 192, 71

Paczyński B., 1998, The Astrophysical Journal Letters, 494, L45

Page D., Lattimer J. M., Prakash M., Steiner A. W., 2004, The Astrophysical Journal Supplement Series, 155, 623

Page D., Prakash M., Lattimer J. M., Steiner A. W., 2011, Physical Review Letters, 106, 081101

Palladino A., Vissani F., 2015, European Physical Journal C, 75, 433

Parke S. J., 1986, Phys. Rev. Lett., 57, 1275

Patrignani C., Group P. D., et al., 2016, Chinese physics C, 40, 100001

Perego A., Rosswog S., Cabezón R. M., Korobkin O., Kaeppeli R., Arcones A., Liebendoerfer M., 2014, Monthly Notices of the Royal Astronomical Society, 443, 3134

Piran T., 1999, Physics Reports, 314, 575

Podsiadlowski P., Mazzali P., Nomoto K., Lazzati D., Cappellaro E., 2004, The Astrophysical Journal, 607, L17

Pontecorvo B., 1968, Sov. Phys. JETP, 26, 165

Popham R., Woosley S. E., Fryer C., 1999, ApJ, 518, 356

Price D. J., Rosswog S., 2006, Science, 312, 719

Rees M. J., Meszaros P., 1992, MNRAS, 258, 41P

Rees M. J., Meszaros P., 1994, ApJL, 430, L93

Reines F., Cowan Jr C. L., Harrison F., McGuire A., Kruse H., 1960, Physical Review, 117, 159

Rosswog S., Liebendörfer M., 2003, MNRAS, 342, 673

Rosswog S., Ramirez-Ruiz E., 2002a, MNRAS, 336, L7

Rosswog S., Ramirez-Ruiz E., 2002b, MNRAS, 336, L7

Rosswog S., Ramirez-Ruiz E., 2003, MNRAS, 343, L36

Rosswog S., Ramirez-Ruiz E., Davies M. B., 2003, MNRAS, 345, 1077

Rowlinson A., O'Brien P., Tanvir N., 2011, in AIP Conference Proceedings. pp 195–198

Ruffert M., Janka H. T., Takahashi K., Schaefer G., 1997, A&A, 319, 122

Sakata S., Inoue T., 1955, Supplement of the Progress of theoretical physics, 1955, 203

Sari R., Piran T., 1997, ApJ, 485, 270

Schwinger J., 1951, Phys. Rev., 82, 664

Sengupta A., 2017

Shahmoradi A., Nemiroff R. J., 2015, Monthly Notices of the Royal Astronomical Society, 451, 126

Shibata M., Taniguchi K., 2006, Phys. Rev. D, 73, 064027

Siegel D. M., Ciolfi R., Rezzolla L., 2014, The Astrophysical Journal Letters, 785, L6

Suzuki Y., 2019, The European Physical Journal C, 79, 1

Tanvir N., Levan A., Fruchter A., Hjorth J., Hounsell R., Wiersema K., Tunnicliffe R., 2013, Nature, 500, 547

Thompson T. A., Chang P., Quataert E., 2004, The Astrophysical Journal, 611, 380

Troja E., Piro L., van Eerten H., et al. 2017, Nature, 000, 1

Tsuruta S., Leung S.-C., Nomoto K., 2018, International Journal of Modern Physics D, 27, 1830004

Tututi E. S., Torres M., D'Olivo J. C., 2002, Phys. Rev. D, 66, 043001

Uso V., 1992, Nature, 357, 472

Vedrenne G. A. J.-L., 2010, Gamma-Ray Bursts: The brightest explosions in the Universe. Springer Praxis Books / Astronomy and Planetary Sciences, Springer

Viganò D., Pons J. A., 2012, Monthly Notices of the Royal Astronomical Society, 425, 2487

Waxman E., 1997, The Astrophysical Journal Letters, 485, L5

Woosley S., 1993a, The Astrophysical Journal, 405, 273

Woosley S., 1993b, The Astrophysical Journal, 405, 273

Zhang B., Meszaros P., 2004, International Journal of Modern Physics A, 19, 2385

Zhang B., Pe'er A., 2009, The Astrophysical Journal, 700, L65

Zhang B., Fan Y. Z., Dyks J., Kobayashi S., Meszaros P., Burrows D. N., Nousek J. A., Gehrels N., 2006, The Astrophysical Journal, 642, 354

Zrake J., MacFadyen A. I., 2013, ApJL, 769, L29

de Salas P. F., Forero D. V., Gariazzo S., Martínez-Miravé P., Mena O., Ternes C. A., Tórtola M., Valle J., 2021, Journal of High Energy Physics, 2021, 1

de Ugarte Postigo A., et al., 2012, Astronomy & Astrophysics, 538, A44